

# Interaction of an oblique shock wave with a pair of parallel vortices: Shock dynamics and mechanism of sound generation

Shuhai Zhang<sup>a)</sup>

*China Aerodynamics Research and Development Center, Mianyang, Sichuan 621000, China*

Yong-Tao Zhang<sup>b)</sup>

*Department of Mathematics, University of Notre Dame, Notre Dame, Indiana 46556*

Chi-Wang Shu<sup>c)</sup>

*Division of Applied Mathematics, Brown University, Providence, Rhode Island 02912*

(Received 10 May 2006; accepted 10 October 2006; published online 12 December 2006)

The interaction between an oblique shock wave and a pair of parallel vortices is simulated systematically through solving the two-dimensional, unsteady compressible Navier-Stokes equations using a fifth order weighted essentially nonoscillatory finite difference scheme. The main purpose of this study is to characterize the flow structure and the mechanism of sound generation in the interaction between an oblique shock wave and a pair of vortices. We study two typical shock waves of Mach number  $M_s=1.2$  and  $M_s=1.05$ , which correspond to two typical shock structures of Mach reflection and regular reflection, respectively, in the problem of shock-vortex interaction. The effects of the strength of the vortices and the geometry parameters are investigated. In addition, we have also considered both cases of passing and colliding vortex pairs. The interaction is classified into four types for the passing case and seven types for the colliding case according to different patterns of the shock structure. Our simulation shows that the sound field is the result of three mechanisms. The first mechanism is related directly to the interaction of the shock wave and the pair of vortices. The second mechanism is related to the coupling process of the vortex pair. The third mechanism is related to the interaction of the reflected shock waves and sound waves. The first mechanism is dominating if the vortex pair is weak. The combination of the first and the second mechanisms is dominating if the vortex pair is of moderate strength. If the vortex pair is strong, the acoustic field is also significantly affected by the interaction of the reflected shock waves and sound waves. © 2006 American Institute of Physics. [DOI: [10.1063/1.2391806](https://doi.org/10.1063/1.2391806)]

## I. INTRODUCTION

Shock waves and vortices are two basic elements of compressible flow. The interaction between them is a common phenomenon and is very important in many applications such as supersonic mixing layers, supersonic jets, and combustion instability. In particular, because a number of shock waves and vortices coexist in supersonic turbulence flow, which is very complicated, the interaction of shock waves and vortices can be seen as a simplified model of shock-turbulence interaction, which is one of the major sources of noise and has received increasing attention.

The interaction of a shock wave and a single vortex is one of the most simplified models of shock-turbulence interaction and has been extensively studied through experiment,<sup>1-3</sup> theoretical analysis,<sup>4-7</sup> and direct numerical simulation.<sup>8-11</sup> A brief summary of a shock-single vortex interaction is given in Zhang *et al.*<sup>12</sup> In addition, Zhang *et al.*<sup>12</sup> studied the interaction of a shock wave and a strong vortex. It is found that the interaction between a shock wave and a strong vortex has a multistage feature. It contains the interaction of the incident shock wave and the initial vortex, of

the reflected shock wave and the deformed vortex, and of the shocklets appearing in the near region of the vortex center and the deformed vortex.

The interaction of a shock wave and a vortex pair is more complicated than that of a shock wave and a single vortex. It contains more complicated physical phenomena including shock wave distortion, shock focusing, crossing, and folding, and has different mechanisms of sound generation. The investigation of this problem can help us better understand the problem of shock-turbulence interaction.<sup>13</sup> Inoue and Hattori<sup>13</sup> studied the flow structure and the near sound field through simulating the interaction of a shock wave with a single vortex or a pair of vortices by solving the two-dimensional Navier-Stokes equations using a sixth order compact scheme.<sup>14</sup> They clarified the basic nature of the near field sound generation. Their study shows that the flow field and the sound waves produced by the interaction have different characteristic features depending on whether the vortex pair moves in the same direction as the shock wave (passing case) or in opposite direction (colliding case). In the interaction between a shock wave and a passing vortex pair, there are four sound waves in the interaction. The essential features of the flow field are not affected by the strength of the shock wave and vortex pair. For the case of a colliding vortex pair, the flow field is affected by the strength of the

<sup>a)</sup>Electronic mail: zhang\_shuhai@tom.com

<sup>b)</sup>Electronic mail: yzhang10@nd.edu

<sup>c)</sup>Electronic mail: shu@dam.brown.edu

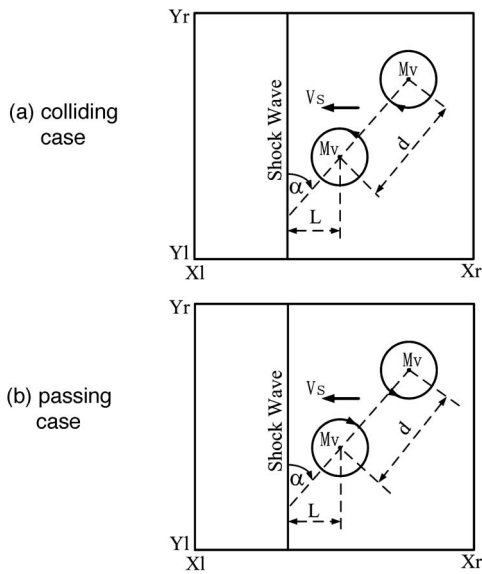


FIG. 1. Schematic diagram of the flow model of colliding and passing cases.

shock wave and vortex pair. The interaction is classified into three types according to different patterns of the shock structure. The first type is a mild interaction without shock focusing. The second type is an intermediate interaction with shock focusing. The third type is a strong interaction with

TABLE I. Parameters of the shock wave and the oblique vortex pair for the simulation.

Case	$M_s$	$M_v$	Re	Case	$M_s$	$M_v$	Re
A	1.2	0.05	800	F	1.05	0.05	800
B	1.2	0.25	800	G	1.05	0.25	800
C	1.2	0.50	800	H	1.05	0.50	800
D	1.2	0.80	800	I	1.05	0.80	800
E	1.2	1.00	800	J	1.05	1.00	800

shock focusing and an additional expansion wave. Three sound waves are observed in the first two types of interaction while there are four sound waves in the third type of interaction. Pirozzoli *et al.*<sup>15</sup> took an extensive parameter study, which contains the shock vortex strength and the distance between the initial vortices, on the interaction of a shock wave with two counter-rotating vortices. For the interaction of a shock wave with a colliding vortex pair, they observe five types of interaction rather than three types in Inoue and Hattori.<sup>13</sup> Two of them, the mild interaction and intermediate interaction, are similar to those in Inoue and Hattori.<sup>13</sup> The other three types contain a weak interaction when the vortex pair is too weak to cause the generation of reflected shock waves, a strong interaction when two pairs of reflected shock waves merge together, and a strong interaction that exhibits a

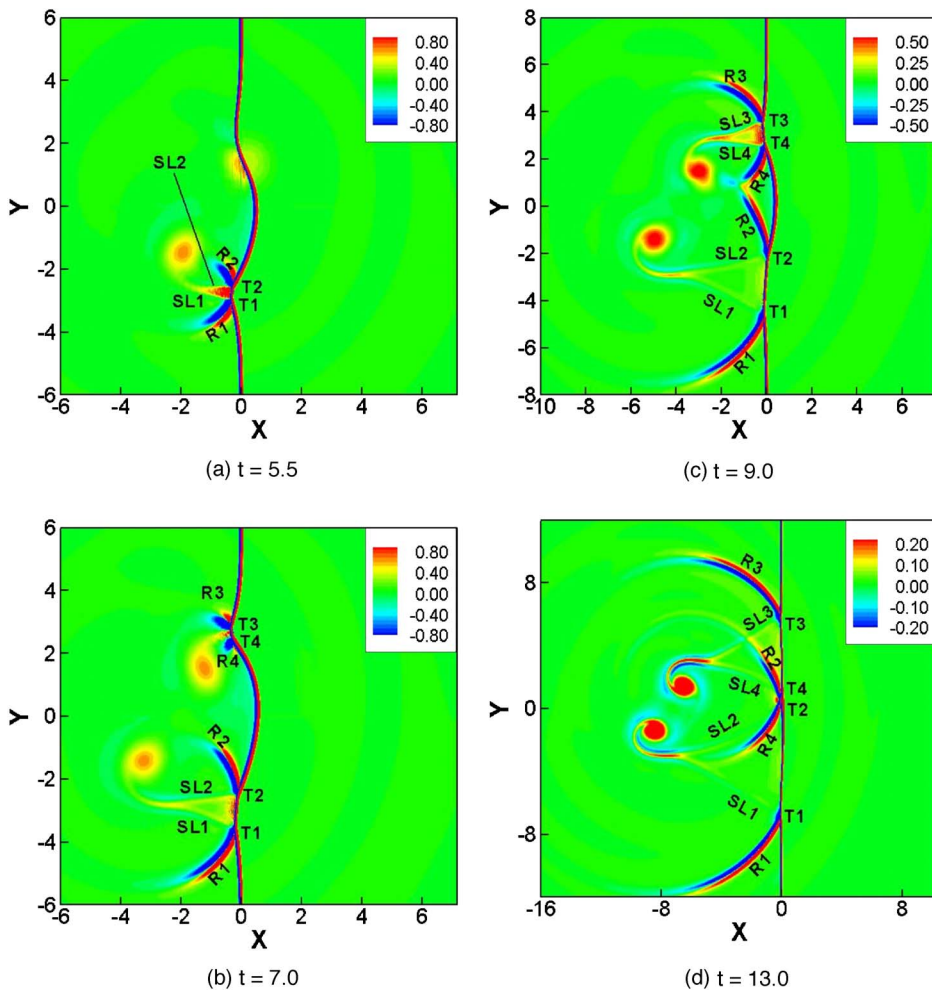


FIG. 2. (Color online) The evolution of the shock structure of an oblique shock and a passing vortex pair interaction,  $M_s=1.2$ ,  $M_v=0.25$ ,  $\alpha=45^\circ$ , and  $L=d=4$ .

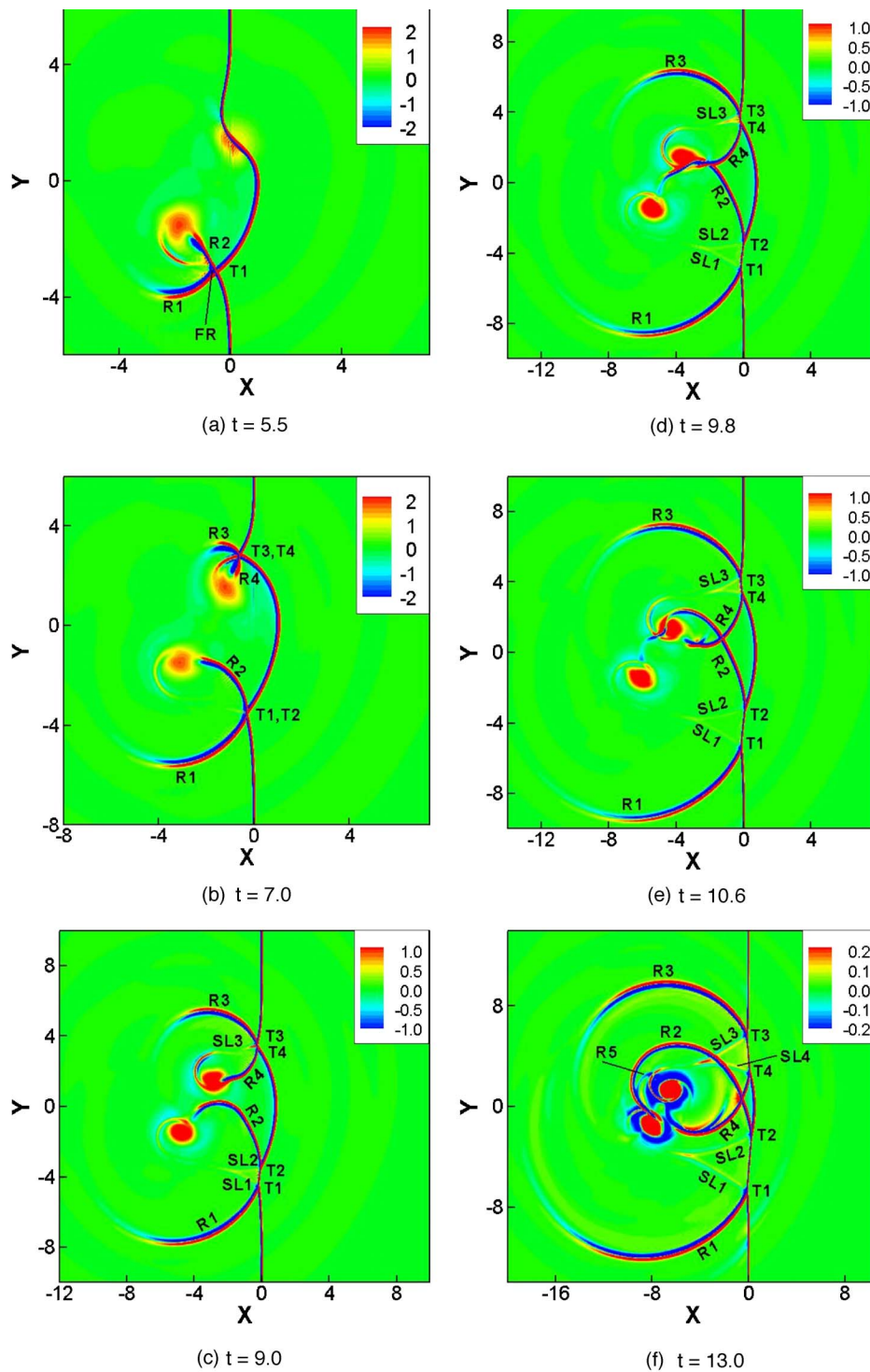


FIG. 3. (Color online) The evolution of the shock structure of an oblique shock and a passing vortex pair interaction,  $M_s=1.2$ ,  $M_v=0.5$ ,  $\alpha=45^\circ$ , and  $L=d=4$ .

regular reflected pattern with a diffracted shock wave between the two vortices. In the passing case, the shock pattern is similar to that in the isolated vortex case, which contains three different types of a weak interaction, Mach reflection, and regular reflection. Four sound waves are observed independently for the colliding vortex pair or the passing vortex pair. There are many differences between the results of Inoue and Hattori<sup>13</sup> and Pirozzoli *et al.*<sup>15</sup> A possible reason is that initial conditions and computational domains are different for the two studies. Inoue *et al.*<sup>16</sup> studied the interaction of a shock wave with two vortices in tandem and in parallel pat-

terns to the shock wave. They found that there is a secondary interaction of the reflected shock wave and the vortices. The reflected shock waves are separated into two parts and it seems that there is another mechanism of sound generation.

In the process of shock vortex pair interaction, there are different physical phenomena and new mechanisms of sound generation compared with a shock and a single vortex interaction. However, previous studies are limited to the vortex pair that is parallel to the plane of the incident shock wave or in tandem. In this case, the flow field is symmetric and some features of the flow structure including mechanisms of sound

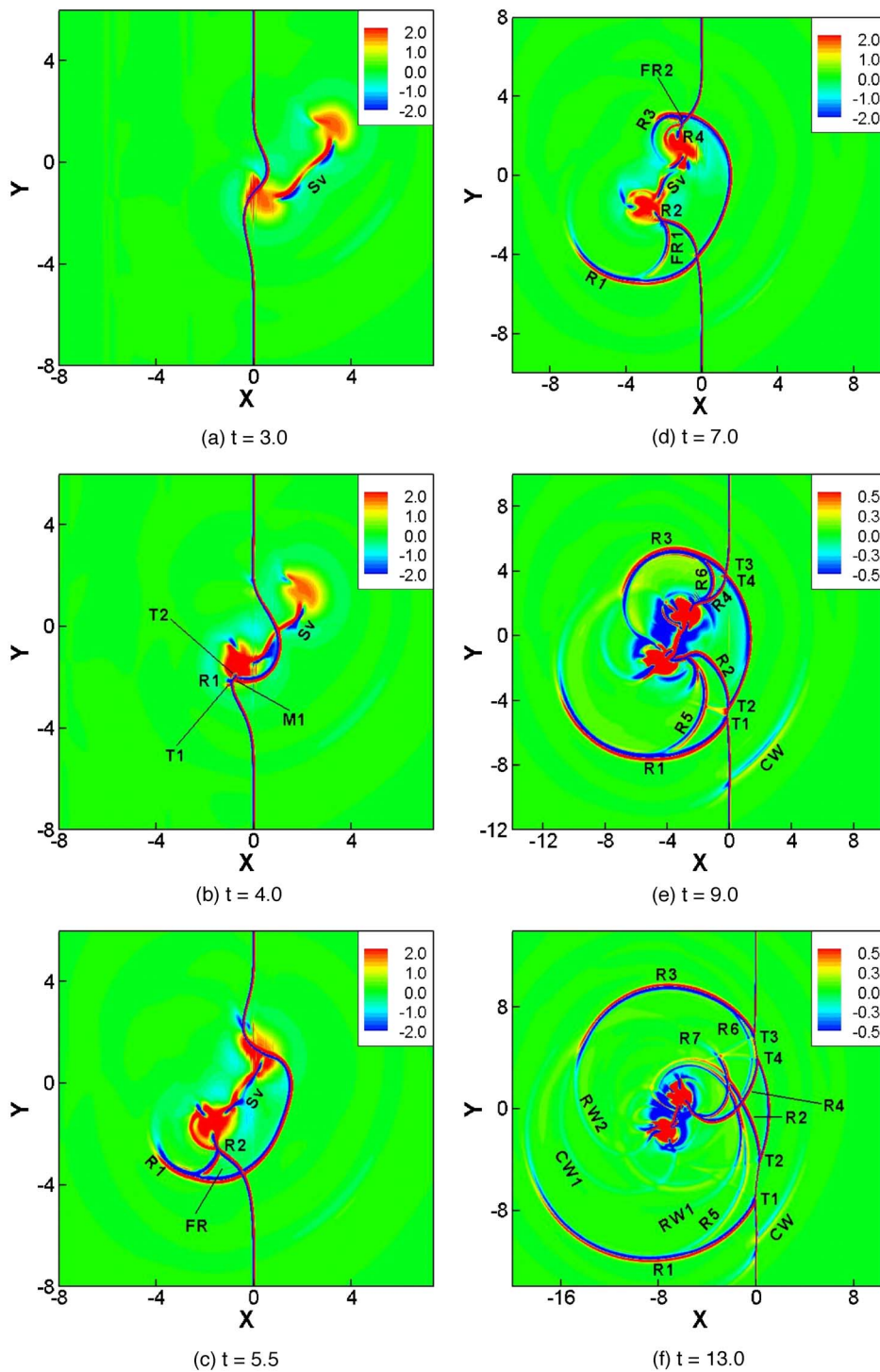


FIG. 4. (Color online) The evolution of the shock structure of an oblique shock and a passing vortex pair interaction,  $M_s=1.2$ ,  $M_v=0.8$ ,  $\alpha=45^\circ$ , and  $L=d=4$ .

generation might be buried. In fact, it is more common in practice that the vortex pair has an angle with the incident shock wave. The supersonic mixing layer, jets, and supersonic turbulence boundary layer are possible examples. There might be some essential differences in the mechanism of sound generation for such unsymmetric cases.

Our purpose in this paper is to study the details of the flow structure and sound generation for the interaction of an oblique shock wave with a vortex pair, through simulating the two-dimensional Navier-Stokes equations using a fifth order weighted essentially nonoscillatory (WENO) scheme.<sup>17</sup>

The effect of the strength of the oblique shock wave and the vortex pair and the geometry parameters are studied systematically. Both cases of the passing vortex pair and colliding vortex pair are considered. Our study shows that there are four different types of interaction for the passing vortex pair and seven different types of interaction for the colliding vortex pair. Some mechanisms of sound generation seem to be essentially different from that of the vortex pair that is parallel to the plane of the incident shock wave. The sound wave results from three different mechanisms including the interaction itself, the coupling process, and the shock-sound

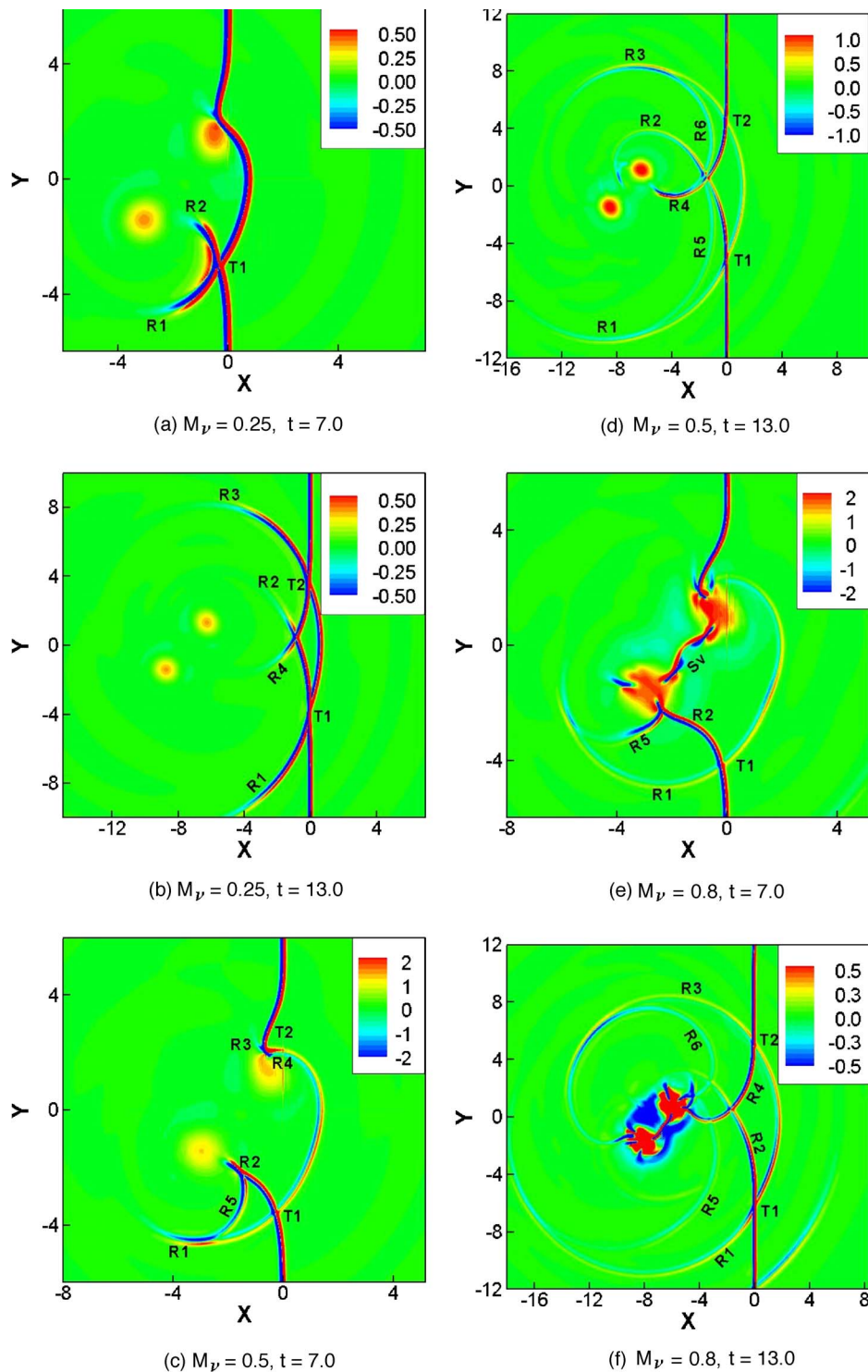


FIG. 5. (Color online) Typical shock structure of an oblique shock and a passing vortex pair interaction,  $M_s = 1.05$ ,  $\alpha = 45^\circ$ , and  $L = d = 4$ .

interaction. The paper is organized as follows: in Sec. II, the physical model and the numerical method are introduced. In Sec. III, we present our numerical results and provide a discussion for the interaction of an oblique shock wave with a vortex pair. The details of the flow structure, the local structure of reflected shock waves, and the mechanism of sound generation are discussed. The last section contains concluding remarks.

## II. MATHEMATICAL FORMULATION AND NUMERICAL PROCEDURE

### A. The physical model

Figure 1 is the schematic diagram of the flow model. The computational domain is prescribed to be rectangular  $x_l < x < x_r$ ,  $y_l < y < y_r$ . In our simulation, we choose two different sizes for the computational domain. One is a smaller domain with  $x_l = -30$ ,  $x_r = 20$ ,  $y_r = -y_l = 20$  for most cases. The

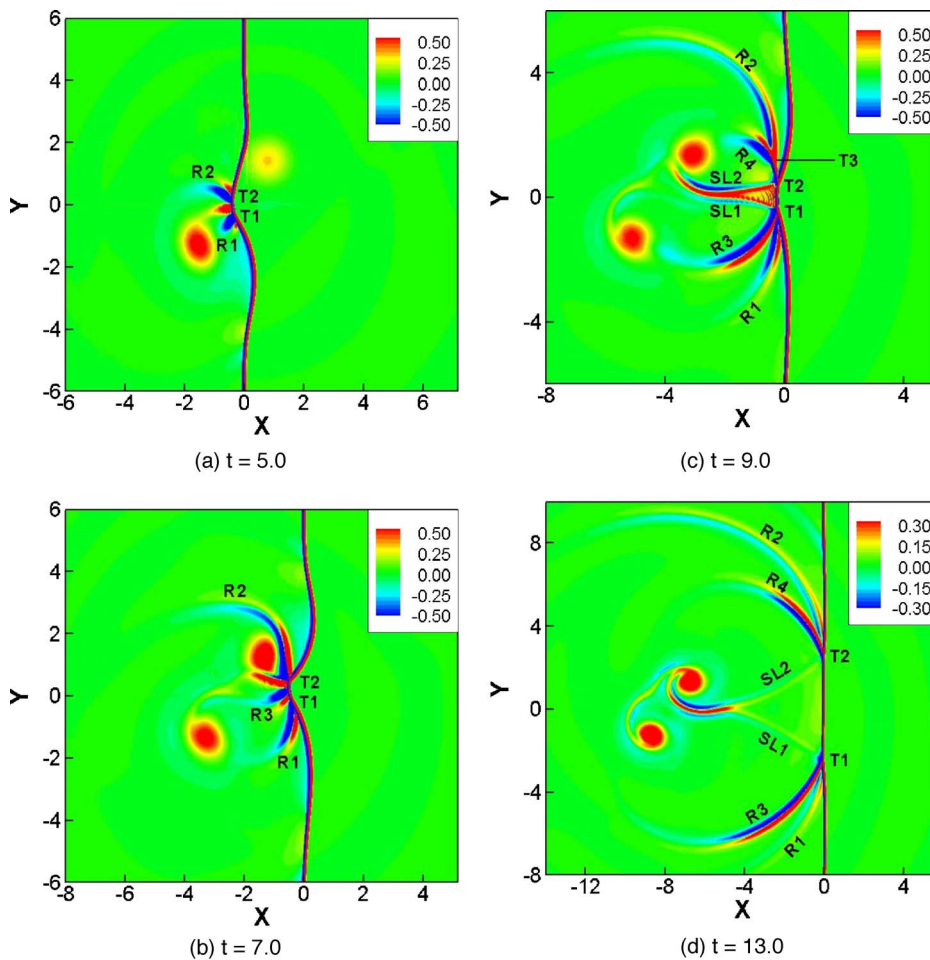


FIG. 6. (Color online) The evolution of the shock structure of an oblique shock and a colliding vortex pair interaction,  $M_s=1.2$ ,  $M_v=0.25$ ,  $\alpha=45^\circ$ , and  $L=d=4$ .

other is a larger domain with  $x_r=-x_l=40$ ,  $y_r=-y_l=30$  to isolate the sound wave generated by the coupling process of the vortex pair. The shock wave is set to be stationary at  $x=0$  in the computation. The vortex pair moves toward the shock at the speed of the shock wave  $V_s$ .  $\alpha$  is the angle between the incident shock wave and the vortex pair. It is prescribed to be  $15^\circ$ ,  $30^\circ$ ,  $45^\circ$ ,  $60^\circ$ , or  $75^\circ$ . As  $\alpha$  approaches  $0^\circ$ , the setup approaches the case that the vortex pair is parallel to the incident shock wave.<sup>16</sup> As  $\alpha$  approaches  $90^\circ$ , it approaches the tandem case.<sup>16</sup> Two different cases of interaction are considered. One is the colliding case shown in Fig. 1(a) in which the  $x$  component of the self-induced velocity of the vortex pair is in the opposite direction to the velocity of the shock wave. The other is the passing case shown in Fig. 1(b) in which the  $x$  component of the self-induced velocity of the vortex pair is in the same direction as the velocity of the shock wave.

The initial flow field is prescribed by the superposition of the flow field produced by each single vortex. The initial location of the first vortex is prescribed to be  $x_d=L$ ,  $y_d=-(d/2)\cos(\alpha)$ , and that of the second vortex to be  $x_u=L+d\sin(\alpha)$ ,  $y_u=(d/2)\cos(\alpha)$ .  $L$  is the initial distance between the first vortex and the incident shock wave.  $d$  is the initial separation distance of the two vortices. Because the effect of the vortex is negligibly small beyond  $r=4$ ,<sup>12,13,15</sup> the initial distance  $L$  is prescribed to be 4 or 20, and the separation distance  $d$  is prescribed to be 4, 6, or 8.

The Mach number of the shock wave is prescribed to be either  $M_s=1.05$  or  $M_s=1.2$ , which correspond to two typical types of interaction: The Mach reflection for  $M_s=1.2$  and regular reflection for  $M_s=1.05$ .<sup>12,13</sup> The Mach number of the vortex  $M_v$ , defined by  $M_v=u_{\theta\max}/a_\infty$ , ranges from 0.05 corresponding to a very weak vortex pair to 1.0 corresponding to a very strong vortex pair. Here,  $u_{\theta\max}$  is the maximum tangential velocity and  $a_\infty$  is the sound speed upstream of the shock wave. In Table I we list the physical parameters used in our simulation to the interaction between the oblique shock waves and the vortex pair. In this table,  $Re$  is the Reynolds number defined by  $Re=\rho_\infty a_\infty R/\mu_\infty$ , where  $\rho_\infty$ ,  $a_\infty$ , and  $\mu_\infty$  are the density, sound speed, and viscosity, respectively, for the mean flow in front of the shock wave, and  $R$  is the radius of the vortex core defined by the distance from the vortex center to the location where the tangential velocity attains its maximum.

## B. The numerical method

The numerical method for this computation is the same as that in Zhang *et al.*,<sup>12</sup> namely the fifth order weighted essentially nonoscillation (WENO) finite difference scheme developed by Jiang and Shu<sup>17</sup> solving the two-dimensional unsteady compressible Navier-Stokes equations. We refer to Ref. 12 for more details.

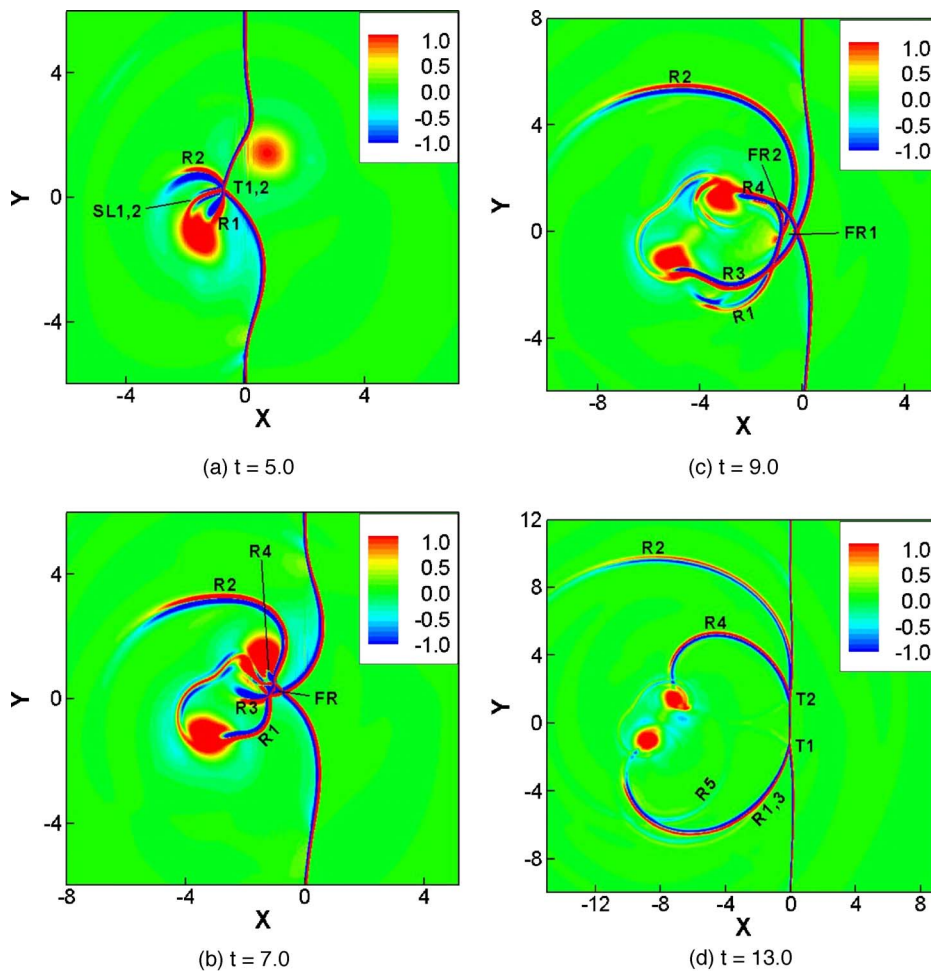


FIG. 7. (Color online) The evolution of the shock structure of an oblique shock and a colliding vortex pair interaction,  $M_s=1.2$ ,  $M_v=0.5$ ,  $\alpha=45^\circ$ , and  $L=d=4$ .

The computational results are obtained on a nonuniform tensor product mesh of  $1280 \times 960$  grid points. The grid transformation is given analytically as

$$x(\xi) = x_i(\xi - \alpha_1 \xi(1 - \xi)e^{-\alpha_2 \xi}), \quad \xi \in [0, 1],$$

$$y(\eta) = y_i(\eta - \beta_1 \eta(1 - \eta)e^{-\beta_2 \eta}), \quad \eta \in [0, 1],$$

where  $\alpha_1=0.905$ ,  $\beta_1=0.92$ , and  $\alpha_2=\beta_2=1.0$ . This grid is refined near  $x=0$  and  $y=0$  and is approximately uniform far away from them. The finest mesh sizes are  $\Delta x \approx 0.00365$  and  $\Delta y \approx 0.0035$  near the coordinate axes, and the coarsest meshes are located near the boundaries, with mesh sizes  $\Delta x \approx 0.05$  and  $\Delta y \approx 0.056$ . This grid guarantees good resolution of the flow field based on our validation tests and previous study on a shock and a strong vortex interaction.<sup>12</sup>

### III. NUMERICAL RESULTS AND DISCUSSION

In this section, computational results for the cases listed in Table I including both the colliding case and passing case are presented. In Sec. III A, the shock structure and its relation with the shock and vortex strengths and the geometry parameters are discussed. The interaction is classified according to the pattern of the shock wave. In Sec. III B, the mechanism of the sound field generated by the interaction is discussed.

#### A. The shock structure

The essential difference between the interaction of an oblique shock wave and a pair of vortices and that of a shock wave and a vortex pair that is parallel to the shock wave is that the flow field of the former case is not symmetric any more, which can reveal new mechanisms of sound generation. The reflected shock waves formed in the interaction of the incident shock wave and one of the two vortices often pass through and interact with the other vortex to form a secondary interaction. Because the shock dynamics is strongly affected by the case of the vortex pair, we discuss the shock structure for the passing vortex pair and the colliding vortex pair separately. In Secs. III A 1 and III A 2, we focus our study on the shock dynamics related with the strength of shock and vortex pair corresponding to the passing vortex pair and colliding vortex pair, respectively, for the specific geometry parameters with  $\alpha=45^\circ$ ,  $d=4$ , and  $L=4$ . Then in Sec. III A 3, we analyze the influence of the geometry parameters to the shock dynamics.

##### 1. Passing vortex pair

There are two features in an oblique shock wave interacting with a passing vortex pair that are not observed in a shock wave interacting with a vortex pair that is parallel to the incident shock wave.<sup>13,15</sup> One feature is the secondary

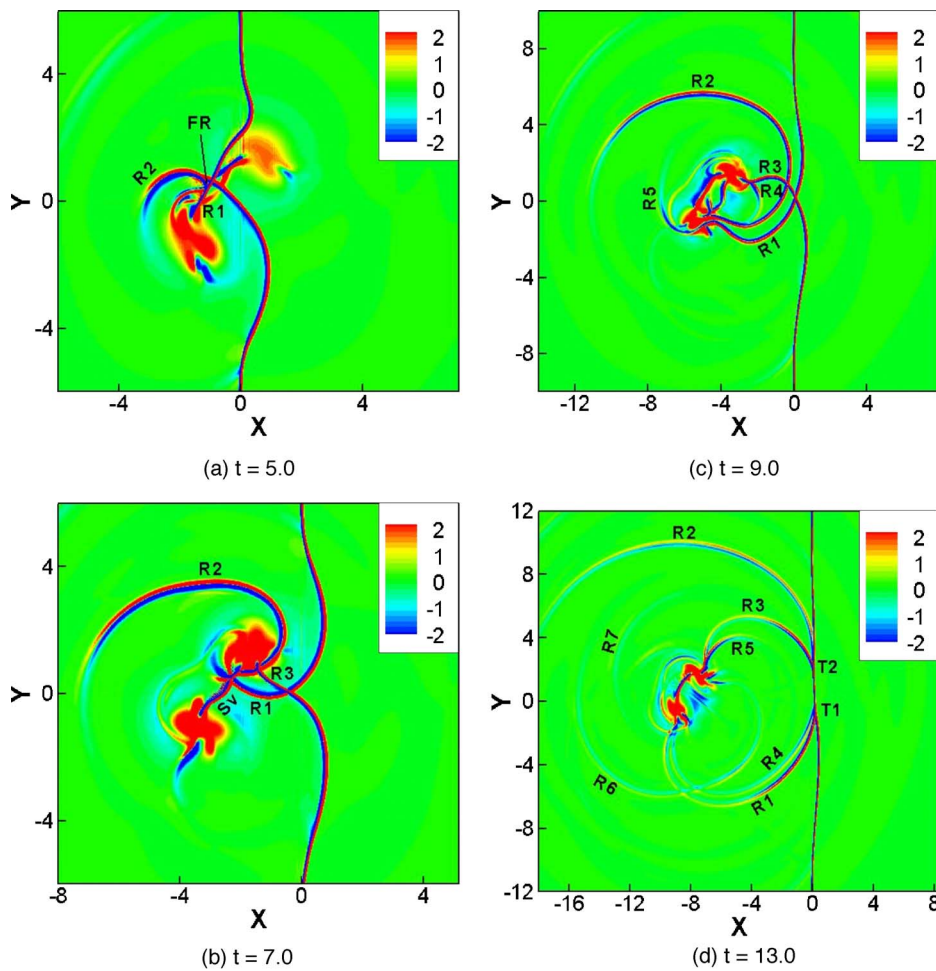


FIG. 8. (Color online) The evolution of the shock structure of an oblique shock and a colliding vortex pair interaction,  $M_s=1.2$ ,  $M_v=0.8$ ,  $\alpha=45^\circ$ , and  $L=d=4$ .

interaction. If the vortex pair is strong, the reflected shock wave formed by the interaction of the incident shock wave and one of the two vortices passes through and interacts with the other vortex to form a secondary interaction. The second feature is that there is another interaction between a bridge-like shock wave, which is formed by the process of vortex coupling, and the vortex pair. This interaction happens before the interaction of the incident shock wave and the vortex pair. To complete the description of the phenomena associated with the interaction of an oblique shock wave with a passing vortex pair, all the interactions during the simulation are discussed and categorized into four types according to different patterns of the shock structure.

The first type (type I) is a weak interaction that is obtained in the interaction of  $M_s=1.2$  and  $M_v=0.05$ , for which we do not show the detailed results here due to the simple shock structure. The vortex pair is too weak to form the reflected shock wave. When the planar shock wave passes the vortex pair, it is distorted to a double S shape. This type is also described by Pirozzoli *et al.*<sup>15</sup> when they studied the interaction of a shock wave and a vortex pair that is parallel to the incident shock wave.

The second type (type II) is a moderate interaction in which the oblique shock vortex pair interaction is similar to the interaction between a shock wave and two isolated vortices. Figure 2 is a typical example of this type for the evolution of the flow structure of  $M_s=1.2$  and  $M_v=0.25$ . The

pictures are shadowgraphs (contours of  $\nabla^2\rho$ ) that are sensitive to the density gradient. They emphasize the discontinuities including the slip lines and are good at providing the main features of the flow field, especially the shock waves and the slip lines. It is observed that after the shock wave passes through the first vortex, two reflected shock waves  $R_1$ ,  $R_2$  appear. A Mach stem between the two triple points  $T_1$  and  $T_2$  and two slip lines  $SL_1$  and  $SL_2$  also appear [see Fig. 2(a)]. The slip lines  $SL_1$  and  $SL_2$  emanate from the triple points  $T_1$  and  $T_2$ , respectively, and spiral into the lower vortex. As the deformed incident shock wave passes through the upper vortex, another pair of reflected shock waves  $R_3$  and  $R_4$  appear. A new Mach stem between the two triple points  $T_3$  and  $T_4$  and two slip lines  $SL_3$  and  $SL_4$  also appear [see Fig. 2(b)]. The slip lines  $SL_3$  and  $SL_4$  emanate from the triple points  $T_3$  and  $T_4$ , respectively, and spiral into the upper vortex. As the interaction develops, the reflected shock wave  $R_2$  moves upward and  $R_4$  moves downward. Later, they cross each other [see Figs. 2(c) and 2(d)]. The developed structure shown in Fig. 2(d) is similar to that in the interaction of a shock wave and a vortex pair that is parallel to the incident shock wave (see Fig. 16 in Ref. 13).

The third type of interaction (type III) is a strong interaction that contains the secondary interaction that is shown in Fig. 3 for the evolution of the flow structure of  $M_s=1.2$  and  $M_v=0.5$ . The reflected shock waves  $R_1$ ,  $R_2$ ,  $R_3$ , and  $R_4$  are stronger than those for  $M_v=0.25$ .  $R_2$  moves upward and

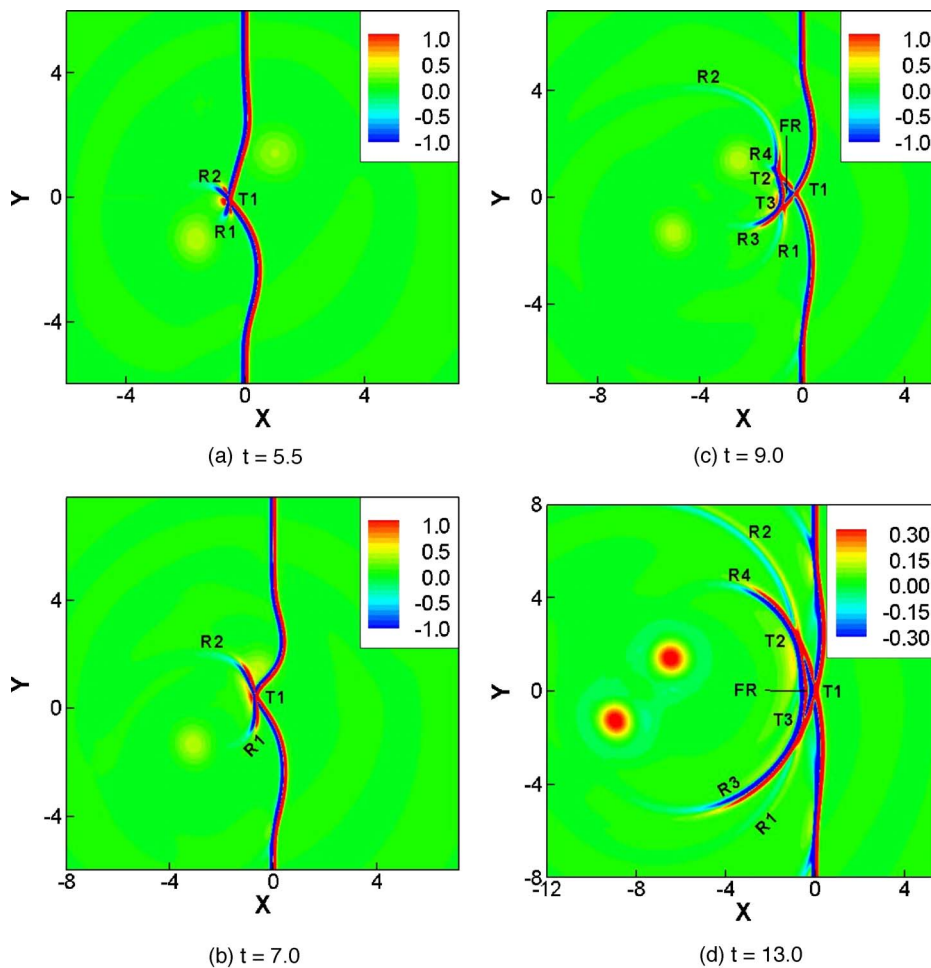


FIG. 9. (Color online) The evolution of the shock structure of an oblique shock and a colliding vortex pair interaction,  $M_s=1.05$ ,  $M_v=0.25$ ,  $\alpha=45^\circ$ , and  $L=d=4$ .

$R_4$  moves downward. They pass through and interact with the upper vortex and the lower vortex, respectively, and form a secondary interaction. As can be seen from Figs. 3(d) and 3(e), the reflected shock wave  $R_2$  is transverse and interacts with the upper vortex. As a result, the reflected shock wave  $R_2$  is distorted into an S shape. After  $R_2$  leaves the upper vortex, a new reflected shock wave  $R_5$  is formed [see Fig. 3(f)]. Therefore, the secondary interaction produces new sound waves.

The fourth type of interaction (type IV) is a strong interaction including the multistage interaction due to the strong vortex pair and an additional interaction due to the vortex coupling effect. Figure 4 is the evolution of the flow field of the vortex  $M_v=0.8$  and  $M_s=1.2$ . Because the vortices are very strong, the coupling effect of the vortex pair becomes significant. The evolution of the coupling process results in a bridge-like shock wave  $SV$  between the two vortices. It interacts with the vortex pair before the incident shock wave reaches the vortex pair [see Fig. 4(a)]. As a result, it is separated by the two vortices and two more shock waves appear in the opposite side of the vortices. This bridge-like shock wave is also observed by Pirozzoli *et al.*<sup>18</sup> when they studied the free evolution of compressible vortex pair. However, when they simulated the interaction of a shock wave and a vortex pair that is parallel to the incident shock wave,<sup>15</sup> they did not observe the shock wave between the two vortices due to the vortex coupling. We suspect that the diffracted shock

wave ( $SN$  in Fig. 10 of Ref. 15) might be the bridge-like shock wave. As the incident shock wave interacts with the first vortex, it also interacts with the bridge-like shock wave [see Figs. 4(b) and 4(c)]. In addition, because the vortices are very strong, the interaction between the incident shock wave and the vortex pair has a multistage feature that is similar to the interaction of a shock wave and a strong vortex.<sup>12</sup> This multistage interaction contains the interaction of the incident shock wave and the initial vortex [see Fig. 4(a)], the reflected shock wave and the deformed vortex [see Figs. 4(c) and 4(d)], and the shocklets appearing in the near region of the vortex center and the deformed vortex [see Figs. 4(d) and 4(e)]. We refer to Zhang *et al.*<sup>12</sup> for more details.

The four types of interaction described above are for  $M_s=1.2$ . For  $M_s=1.05$ , the flow structures are quite similar to the corresponding patterns of  $M_s=1.2$ . Figure 5 displays typical patterns of the flow structure for the shock Mach number  $M_s=1.05$  and typical vortex Mach numbers. The key difference is the structure of the incident shock wave with a regular reflection, which is the same as that in a shock wave and a single vortex interaction.<sup>12,13,19</sup>

## 2. Colliding vortex pair

For a colliding vortex pair, the flow structure, especially the shock structure, is more sensitive to the strengths of the shock wave and the vortex than those for the passing vortex

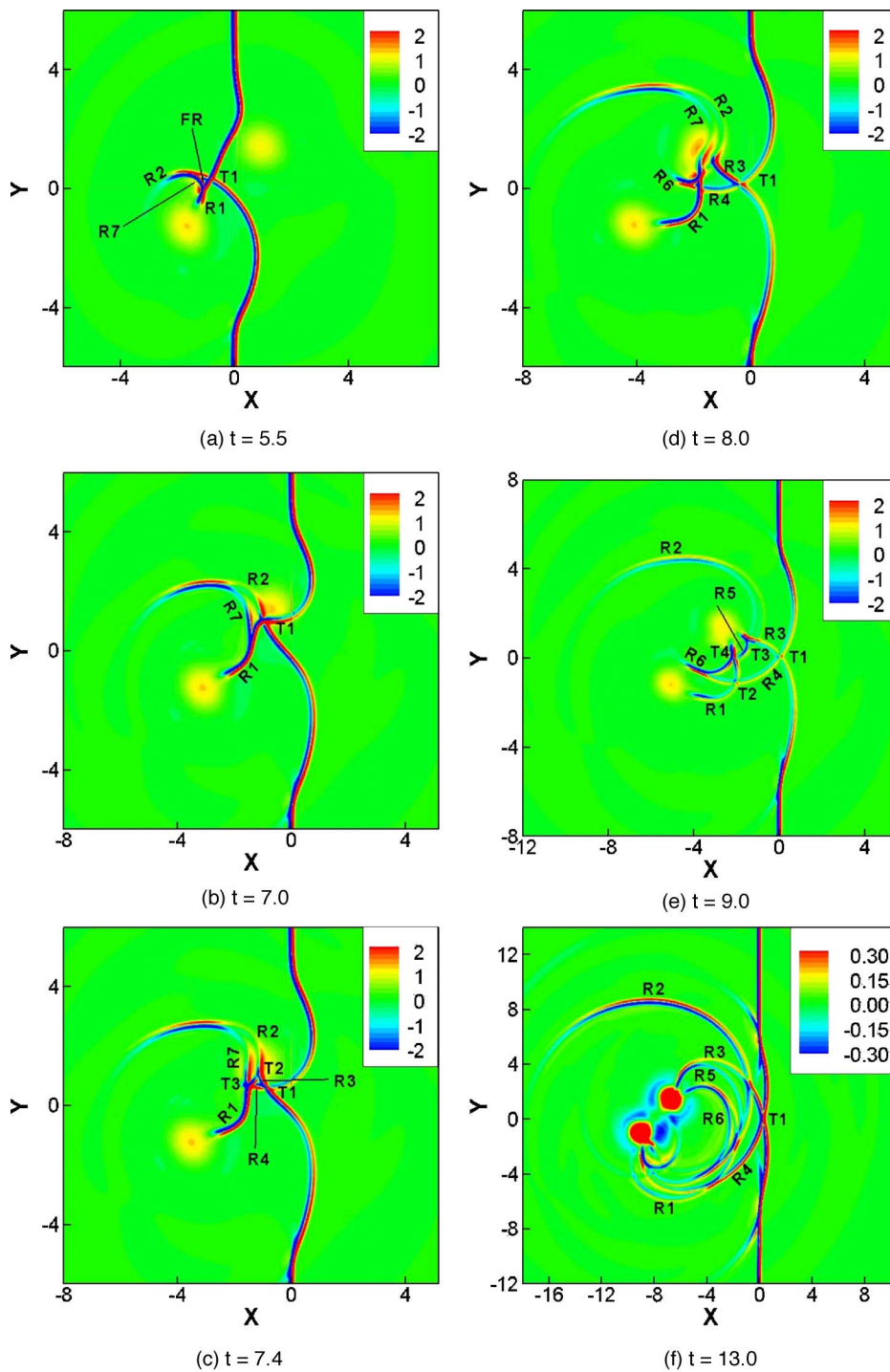


FIG. 10. (Color online) The evolution of the shock structure of an oblique shock and a colliding vortex pair interaction,  $M_s=1.05$ ,  $M_v=0.5$ ,  $\alpha=45^\circ$ , and  $L=d=4$ .

pair. Due to the counterclockwise rotation of the first vortex, one of the two reflected shock waves, which is formed in the interaction of the incident shock wave and the first vortex, always passes through the upper vortex just after the deformed incident shock wave passes it. The secondary interaction between the reflected shock wave and the upper vortex merges together with the interaction of the distorted incident shock wave and the upper vortex. This is an essential difference with that of the interaction between a shock wave and a colliding vortex pair that is parallel to the incident shock wave. In general, the interaction can be classified into the following seven types.

The first type of interaction (type I) is a weak interaction similar to that in the passing vortex pair in which the vortex pair is too weak to form the reflected shock wave. After the incident shock wave passes the vortex pair, it is only distorted into a double S shape. This type happens when  $M_v=0.05$  (not reported here due to the simple shock structure).

The second type of interaction is a moderate interaction (type II), which is the basic interaction of an oblique shock wave and a colliding vortex pair shown in Fig. 6 for the evolution of the flow structure of  $M_s=1.2$  and  $M_v=0.25$ . It is observed that two reflected shock waves  $R_1$  and  $R_2$  are

formed after the incident shock wave passes through the first vortex. These two reflected shock waves  $R_1$  and  $R_2$  are located between the two vortices shown in Fig. 6(a).  $R_1$  moves downward and  $R_2$  moves upward. As time increases, the deformed incident shock wave and the reflected shock waves  $R_1$  and  $R_2$  move toward the upper vortex. Later, the deformed incident shock wave and the reflected shock wave  $R_2$  pass through the upper vortex almost at the same time. The first interaction between the deformed incident shock wave and the upper vortex and the secondary interaction between the reflected shock wave  $R_2$  and the upper vortex merge together [see Fig. 6(b)]. As a result, two more reflected shock waves  $R_3$  and  $R_4$  are formed. The root of  $R_4$  merges with the reflected shock wave  $R_2$ . It seems that there is another triple point  $T_3$  apart from the triple point  $T_2$ .  $T_3$  moves toward  $T_2$  and finally merges together with  $T_2$ .

The third type of interaction (type III) is a strong interaction with shock focusing, folding, and crossing. This type is shown in Fig. 7 for the evolution of the flow structure of  $M_s=1.2$  and  $M_v=0.5$ . When the distorted incident shock wave and the reflected shock wave  $R_2$  pass through the upper vortex, both the incident shock wave and the reflected shock wave  $R_2$  are distorted. Because the incident shock wave is deformed by the first interaction of the incident shock wave and the first vortex, the interaction between the deformed incident shock wave and the upper vortex takes the pattern of a regular reflection that can be seen in Fig. 7(b). At the same time, a new triple point  $T_3$  and a new reflected shock wave  $R_4$  are formed in the secondary interaction between the reflected shock wave  $R_2$  and the upper vortex. As a result, a shock focusing region  $FR$  appears. As the interaction further develops, the reflected shock wave  $R_4$  becomes stronger and longer. The tip of the reflected shock wave  $R_4$  touches and interacts with the upper vortex [see Fig. 7(c)]. The reflected shock waves  $R_1$  and  $R_3$  pass through the lower vortex successively and interact with the lower vortex. The reflected shock waves  $R_1$ ,  $R_2$ ,  $R_3$ , and  $R_4$  cross each other to form a shock crossing region including two shock focusing regions  $FR_1$  and  $FR_2$ . Finally,  $R_1$  and  $R_3$  merge together and the shock focusing regions disappear.

The fourth type of interaction (type IV) is a strong interaction including the multistage interaction and an additional interaction due to the coupling effect. This type happens at  $M_s=1.2$ ,  $M_v=0.8$  shown in Fig. 8. For this type, the vortex pair is very strong. The vortex coupling effect results in a bridge-like shock wave  $SV$  between the two vortices. It interacts with the vortex pair first similar to that in the passing vortex pair. As the deformed incident shock wave and the reflected shock wave  $R_2$  interact with the upper vortex, they also interact with the bridge-like shock wave. In addition, because the vortex is strong, there is also the multistage interaction between the reflected shock wave and the deformed vortex and between the shocklets and the deformed vortex, which is similar to that of a shock wave and a single strong vortex.<sup>12</sup>

The fifth type of interaction (type V) is a strong interaction including the shock focusing. This type is shown in Fig. 9 for the evolution of the flow structure of  $M_s=1.05$  and  $M_v=0.25$ . Due to the difference of the incident shock wave

with those in the previous four types of interaction, the deformation of the incident shock wave is a regular reflection, which has also been reported in previous studies.<sup>12,13,15</sup> This is an essential difference with that of the case  $M_s=1.2$ . In this case, the secondary interaction between the reflected shock wave  $R_2$  and the upper vortex generates a shock focusing region just after the reflected shock wave  $R_2$  passes the upper vortex [see Fig. 9(c)]. This shock focusing region is the same as that in the experiment study of Sturtevant and Kulkarny<sup>20</sup> and the numerical study in Refs. 12, 13, and 15. The flow keeps this pattern for a very long time as shown in Fig. 9(d).

The sixth type of interaction (type VI) is a strong interaction with a shock focusing region interacting with the upper vortex. This type is shown in Fig. 10 for the evolution of the shock structure for  $M_s=1.05$  and  $M_v=0.5$ . As can be seen from Fig. 10(a), after the incident shock wave passes the first vortex, one of the reflected shock waves  $R_1$  interacts with the first vortex and a new reflected shock wave  $R_7$  is formed. The tip of the reflected shock wave  $R_7$  merges with the other reflected shock wave  $R_2$  and forms a shock focusing region  $FR$ . This shock focusing region is described in detail by Zhang *et al.*<sup>12</sup> for the interaction of a shock wave and a single strong vortex. As the interaction develops, the deformed incident shock wave and the shock focusing region  $FR$  pass through the upper vortex successively [Figs. 10(b)–10(d)]. As a result, the shock waves are distorted again. The upper part is accelerated whereas the lower part is decelerated. The interaction between the distorted incident shock wave and the upper vortex results in the formation of two reflected shock waves  $R_3$  and  $R_4$  [Fig. 10(c)]. At the same time, the reflected shock waves  $R_2$  and  $R_7$  interact with the upper vortex, which results in the formation of two more reflected shock waves  $R_5$ ,  $R_6$ , and two more triple points  $T_3$  and  $T_4$ . As a result, there appears a complicated shock focusing region including the reflected shock waves  $R_3$ ,  $R_4$ ,  $R_5$ , and  $R_6$  [Fig. 10(e)]. These shocks develop into a complex shock wave structure shown in Fig. 10(f).

As we further increase  $M_v$ , the effect of vortex coupling becomes significant. There is a bridge-like shock wave  $SV$  between the two vortices that interacts with the vortex pair first before the incident shock wave reaches the vortex pair. The deformed incident shock wave and the shock focusing region  $FR$  interact with the bridge-like shock wave  $SV$  and the upper vortex. In addition, there is a multistage interaction of a shock wave and a strong vortex, which is the same as those in type IV. The combination of these three interactions becomes our seventh type (type VII) of interaction with the effect of vortex coupling and multistage feature for a strong vortex. It occurs when  $M_v \geq 0.8$  shown in Fig. 11 for  $M_v=0.8$ .

### 3. The influence of the geometry parameters

To verify the generality of the shock dynamics categorized on the previous subsections and link them with the previous studies,<sup>15,16</sup> we study the influence of the geometry parameters, including the angle  $\alpha$  of the oblique shock wave,

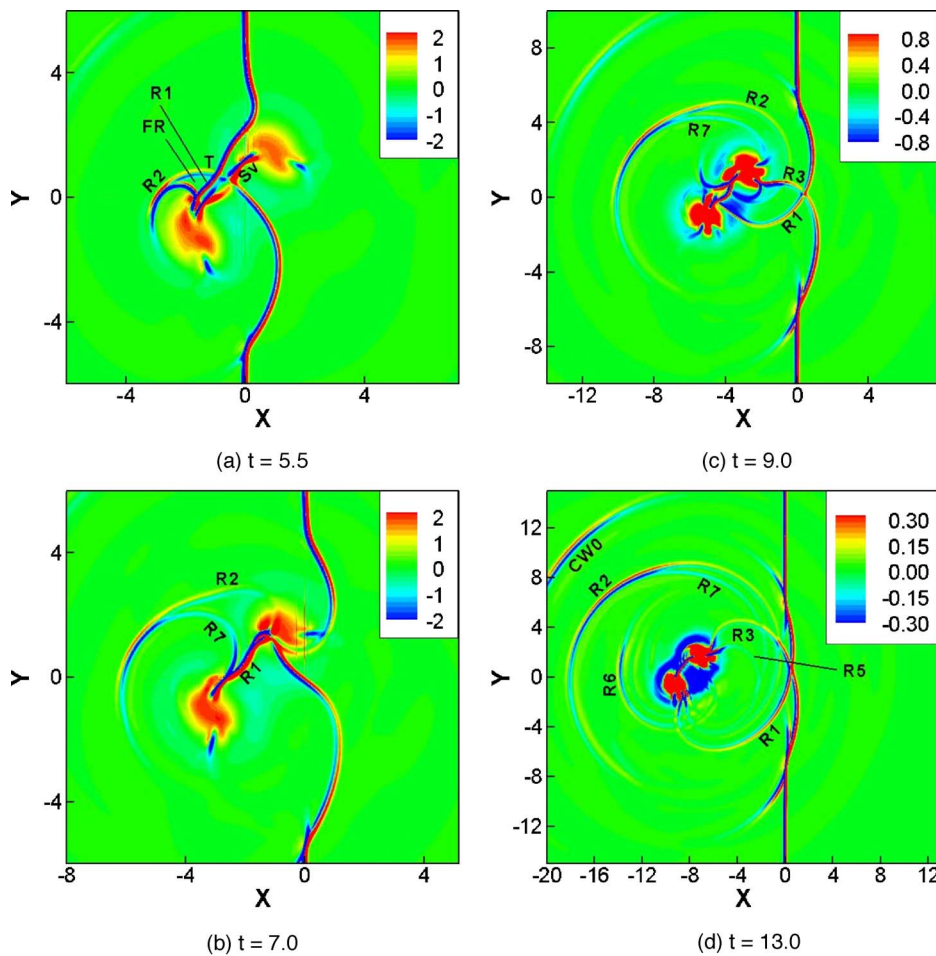


FIG. 11. (Color online) The evolution of the shock structure of an oblique shock and a colliding vortex pair interaction,  $M_s=1.05$ ,  $M_v=0.8$ ,  $\alpha=45^\circ$ , and  $L=d=4$ .

the initial distance  $L$  between the vortex pair and the incident shock wave, and the initial separation distance  $d$  of the two vortices.

Besides the case of  $\alpha=45^\circ$  reported before, we let the angle  $\alpha$  vary from  $15^\circ$ ,  $30^\circ$ ,  $60^\circ$ , to  $75^\circ$ . For the passing case, the shock Mach number is set to be  $M_s=1.2$  and the strength of the vortex pair is  $M_v=0.5$  and  $0.8$ . For the colliding case, the shock Mach number is set to be  $M_s=1.05$ . The strength of the vortex pair is  $M_v=0.25$  and  $0.5$ . Figure 12 shows the typical shock structure for the passing case of  $M_s=1.2$  and  $M_v=0.5$ . We can observe that the shock structure does not change significantly as  $\alpha$  varies from  $15^\circ$  to  $75^\circ$ . They are essentially the same as those of  $\alpha=45^\circ$  shown in Fig. 3. The only difference is the time for the secondary interaction to happen. For example, in the case of  $\alpha=15^\circ$ , the reflected shock wave  $R2$  has not reached the second vortex at  $t=9$  [see Fig. 12(a)]. In the case of  $\alpha=75^\circ$ , it is transverse and interacts with the second vortex at  $t=9$  [see in Fig. 12(g)]. As  $\alpha$  approaches  $0^\circ$ , the developed shock structure approaches the symmetric feature shown in Fig. 12(b), which is the same to that in the parallel case of Fig. 19(a) in Ref. 13. As  $\alpha$  increases, the asymmetric feature becomes stronger. Figure 13 is the typical shock structure for the colliding interaction of  $M_s=1.05$  and  $M_v=0.5$ . Comparing with those of the  $\alpha=45^\circ$  case shown in Fig. 10, we observe that the interaction of the  $\alpha=30^\circ$  and  $60^\circ$  cases has the same multishock focusing structure. For example, Fig. 13(c) corresponds to Fig. 10(c),

Fig. 13(d) corresponds to Fig. 10(e), Fig. 13(e) corresponds to Fig. 10(b), and Fig. 13(f) corresponds to Fig. 10(e). As  $\alpha$  decreases, the multishock focusing structure becomes narrower in the  $x$  direction and finally becomes symmetric to the  $x$  axis as in the parallel case<sup>16</sup> when  $\alpha=0^\circ$ . As  $\alpha$  approaches  $90^\circ$ , it becomes similar to the tandem case. For example, Fig. 13(g) corresponds to Fig. 5(a) in Ref. 16. Both the parallel and the tandem cases were studied extensively by Inoue *et al.*<sup>16</sup>

The initial distance  $L$  does not seem to have a significant influence on the shock structure if it is larger than 4. Figure 14 is the typical flow field for the passing vortex pair of  $M_v=0.25$  and  $0.8$  with the initial distance  $L=20$ . The shock Mach number is  $M_s=1.2$ . The angle is  $\alpha=45^\circ$  and the initial separation distance is  $d=4$ . When they move to  $t=15$ , the positions of the two vortices are  $(2.17, -1.44)$  and  $(4.84, 1.24)$  in the case of  $M_v=0.25$  and  $(3.02, -1.82)$  and  $(5.22, 0.37)$  in the case of  $M_v=0.8$ . The separation distance becomes 3.78 and 3.11, respectively. In the case of the weaker vortex pair  $M_v=0.25$ , the separation distance at  $t=15$  becomes slightly smaller than the initial separation distance due to the effect of vortex coupling. In the stronger vortex pair case  $M_v=0.8$ , the separation distance at  $t=15$  becomes much smaller than the initial separation distance due to the effect of vortex coupling and the interaction of the bridge-like shock and the vortex pair. However, the angle

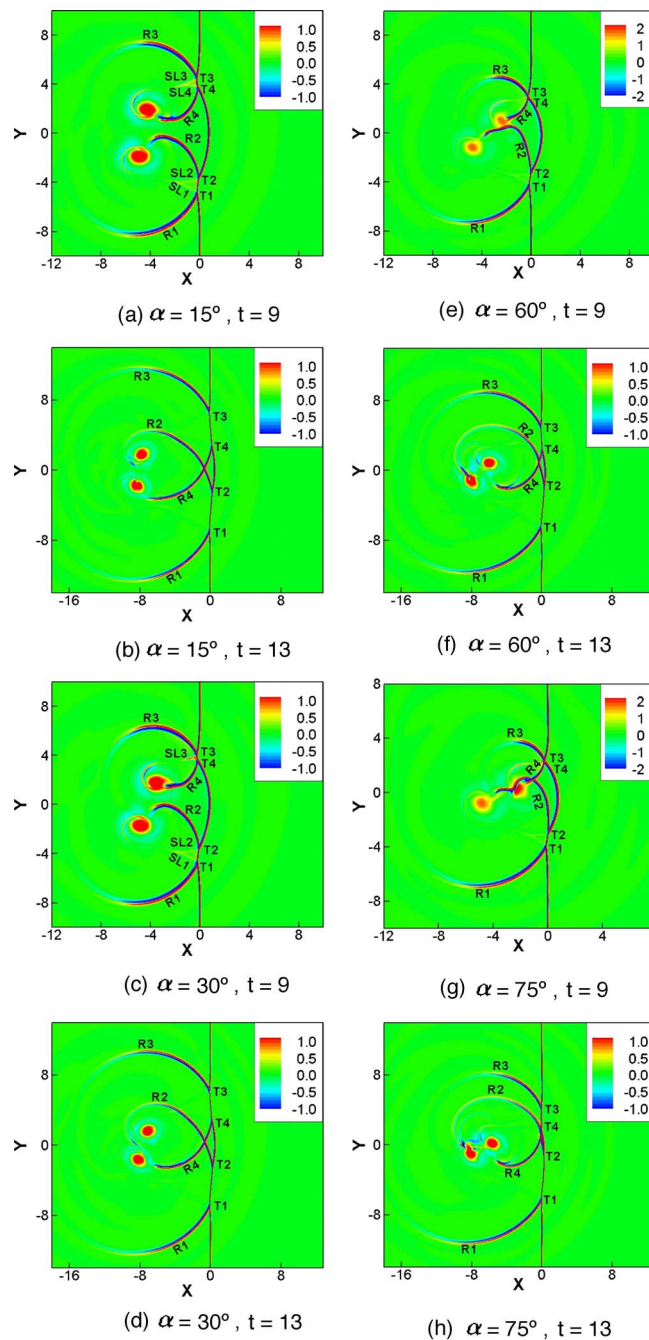


FIG. 12. (Color online) The typical shock structure of an oblique shock and a passing vortex pair interaction at different  $\alpha$ ,  $M_s=1.2$ ,  $M_v=0.5$ ,  $L=d=4$ .

between the incident shock wave and the connecting line of two vortex centers does not change. They are  $45.08^\circ$  and  $44.9^\circ$  correspondingly. The developed shock structure at  $t=25$  shown in Fig. 14 have the same configuration with those of initial distance  $L=4$  shown in Figs. 2 and 4.

The separation distance  $d$  does influence the coupling effect of the two vortices. As the separation distance increases, the coupling between the two vortices becomes weaker. When the separation distance is larger than 6, they will behave as isolated vortices which result in the disappearance of the bridge-like shock wave  $SV$ . In addition, because the distance between the two vortices becomes large, the

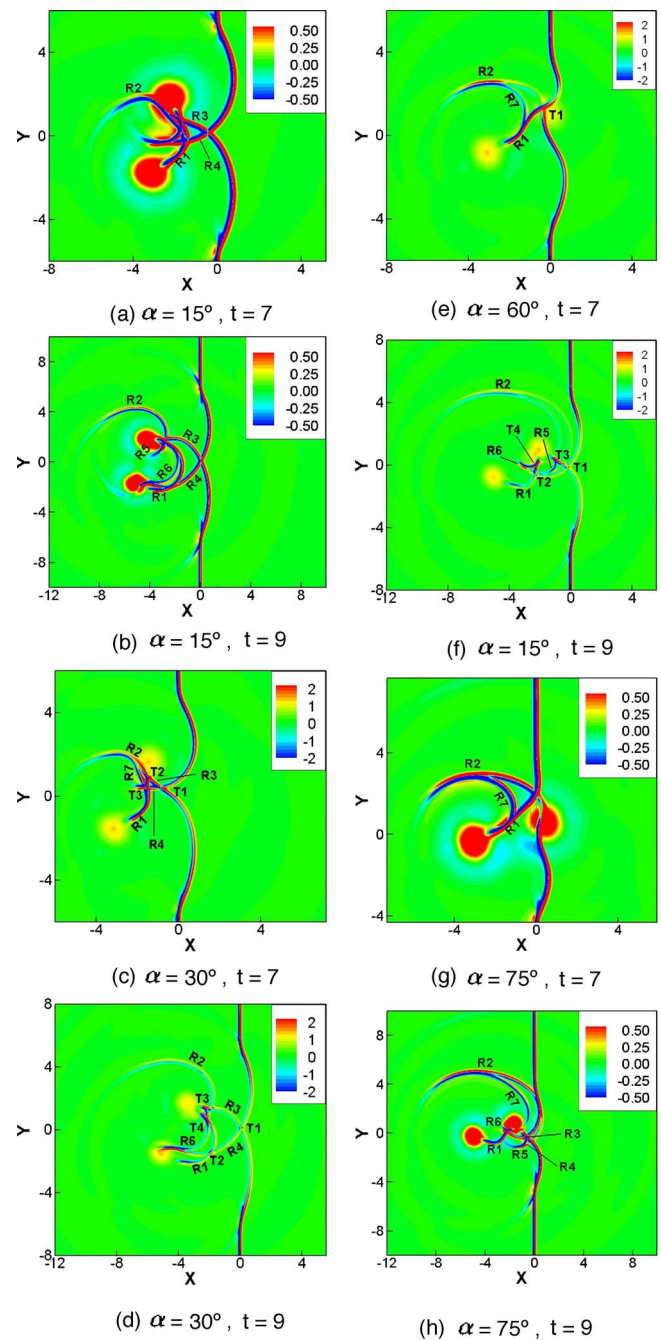


FIG. 13. (Color online) The typical shock structure of an oblique shock and a colliding vortex pair interaction at different  $\alpha$ ,  $M_s=1.05$ ,  $M_v=0.5$ ,  $L=d=4$ .

secondary interaction between the reflected shock wave or the shock focusing region and the second vortex will be affected. Figure 15 contains the typical shock structure for the passing vortex pair of  $M_v=0.5$  at the separation distance  $d=6$  and 8. The shock Mach number is  $M_s=1.2$ . The angle  $\alpha$  is  $45^\circ$  and the initial distance is  $L=4$ . Compared with those of the  $d=4$  case shown in Fig. 3, they have the same shock structure except for the difference of the time for the secondary interaction between the reflected shock wave  $R_2$  and the second vortex to happen. Figure 16 is the typical shock structure of the interaction of an oblique shock wave  $M_s=1.2$  and

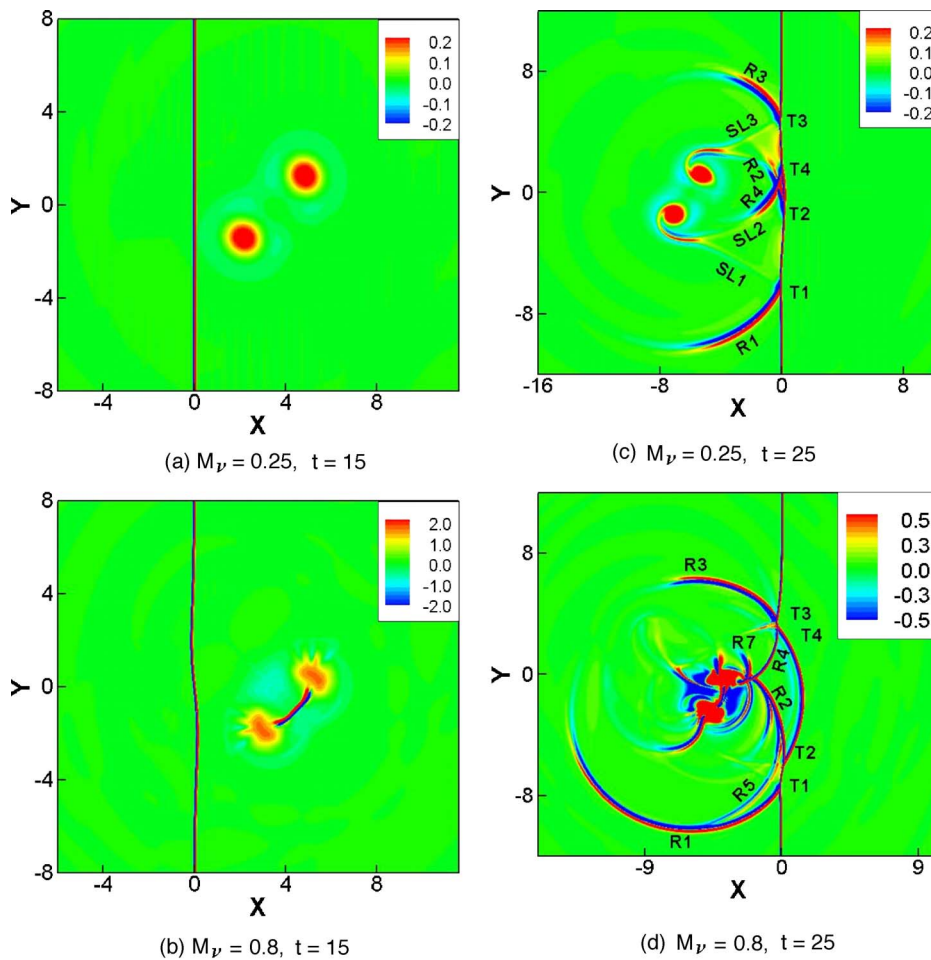


FIG. 14. (Color online) The shock structure of an oblique shock and a passing vortex pair interaction of  $M_s = 1.2$  with the initial distance  $L=20$ ,  $\alpha=45^\circ$ , and  $d=4$ .

a strong vortex pair  $M_v=0.8$ . In this case, the bridge-like shock wave  $SV$  does not appear. It behaves as the interaction of the shock wave with two isolated vortices, which are similar with that in the interaction of an oblique shock wave and a weaker vortex pair in a shorter separation distance shown in Figs. 3 and 15. The only difference is that there is more than one reflected shock wave, namely  $R_2$ ,  $R_5$ , and  $R_7$ , which successively interact with the second vortex.

## B. Mechanism of sound generation

The generation and propagation of sound waves is the most interesting phenomenon in the problem of shock vortex interaction. The generation of sound waves in the interaction of a shock wave and a single vortex has been studied extensively in Refs. 12, 13, and 19, as well as the basic structure of sound waves in the interaction of a shock wave and a vortex pair that is parallel to the incident shock wave in Refs. 13 and 15. However, in the interaction of an oblique shock wave and a pair of vortices, there are different mechanisms of sound generation which contain the interaction itself, the effect of the vortex coupling process, and shock-sound interaction.

### 1. Mechanism of sound generation in the interaction of an oblique shock and a pair of vortices

Figure 17 is the evolution of the sound wave, which is generated in the interaction of an oblique shock wave of Mach number  $M_s=1.2$  and a passing vortex pair of

$M_v=0.05$ . The angle of the shock wave and the connecting line between the centers of two vortices is  $\alpha=45^\circ$ . Both the initial distance and the separation distance are 4. In this figure, the symbol  $\oplus$  denotes the compression region ( $\Delta p > 0$ ) while  $\ominus$  denotes the rarefaction region ( $\Delta p < 0$ ). This vortex pair is very weak so that the effect of the vortex coupling and shock-sound interaction can be neglected.

As can be seen from Figs. 17(a) and 17(b), immediately after the incident shock wave touches the first vortex, a compressible region and a rarefaction region appear downstream of the incident shock wave. Because the vortex pair is very weak, the distortion of the incident shock wave is not significant. As the interaction develops, one more compressible region and one more rarefaction region appear. These four alternating compressible and rarefaction regions become the precursor generated by the first interaction of the incident shock wave and the first vortex. This process is quite similar to that in the interaction of a shock wave and a single vortex.<sup>13</sup> As can be seen from Fig. 17(c), when the incident shock wave touches the edge of the second vortex, there is a pair that is composed of a compressible region and a rarefaction region. Because the second vortex is counterclockwise, the compressible region is on the upper part and the rarefaction region is on the lower part. This is part of the precursor of the second interaction of the deformed incident shock wave and the second vortex. It is the same in sign with the precursor generated by the first interaction of the incident

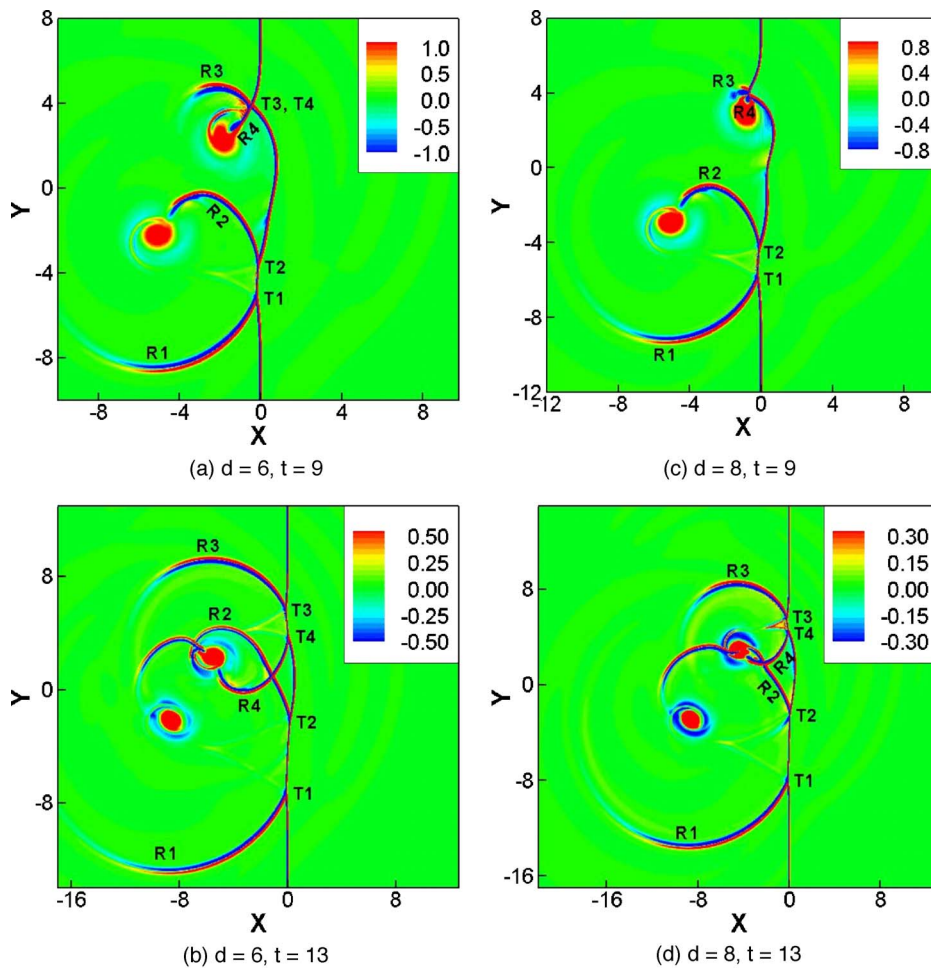


FIG. 15. (Color online) The shock structure of an oblique shock and a passing vortex pair interaction with different separation distance.  $M_s=1.2$ ,  $M_v=0.5$ ,  $\alpha=45^\circ$ ,  $L=4$ .

shock wave and the first vortex. The two sound waves merge together. When the incident shock wave enters the second vortex, there appears one more rarefaction region in the top right region of the precursor, which can be seen in Fig. 17(d). These five alternating compressible and rarefaction regions combine together to form the precursor of the oblique shock wave and the vortex pair interaction. After the incident shock wave leaves the vortex pair, three more sound waves appear successively behind the precursor.

There are two features that are essentially different between the sound waves in the interaction of an oblique shock wave and a vortex pair and that of a shock wave and a vortex pair that is parallel to the incident shock wave. (1) There are double cells in the second sound wave in the interaction of an oblique shock wave and a vortex pair rather than a single cell in the interaction of a shock wave and a vortex pair that is parallel to the incident shock wave. (2) For the interaction of an oblique shock wave and a vortex pair, the four sound waves propagate radially outward from different centers. The precursor radiates outward from the center of the first vortex. The second sound wave radiates outward from the middle point of the two vortices. The third and the fourth sound waves radiate outward from the center of the second vortex. These two features indicate that there is a merging mechanism of sound waves.

As can be seen from Fig. 17(f), the left bottom part (the rarefaction region in the negative  $y$  region) of the second

sound wave has a double cell structure that is not observed in the simulation of Inoue and Hattori<sup>13</sup> and Pirozzoli *et al.*<sup>15</sup> In fact, the vortex pair is very weak. The interaction of an oblique shock wave and a weak vortex pair is similar to the interaction of a shock wave and two isolated counter rotating vortices. It is well known that the interaction of a shock wave and a single vortex produces three sound waves,<sup>12,13,19</sup> hence we can assume that there are six sound waves after a shock wave interacts with two isolated vortices. Because the two vortices are very close, some of the sound waves merge together resulting in only four observed sound waves. The precursor [marked by  $F$  in Fig. 17(f)] mainly comes from the precursor generated by the first interaction of the incident shock wave and the first vortex. It radiates outward from the center of the first vortex. The second sound wave [marked by  $S$  in Fig. 17(f)] results from the merging of the second sound wave generated by the interaction of the incident shock wave and the first vortex and the precursor generated in the second interaction of the deformed incident shock wave and the second vortex. When the precursor, which is generated by the interaction of the incident shock wave and the second vortex, propagates outward from the center of the second vortex, the lower rarefaction part passes through the first vortex and catches up with the second sound wave generated by the interaction of the incident shock wave and the first vortex. As a result, they merge together to form the second sound wave of the interaction of the oblique shock wave and the vortex

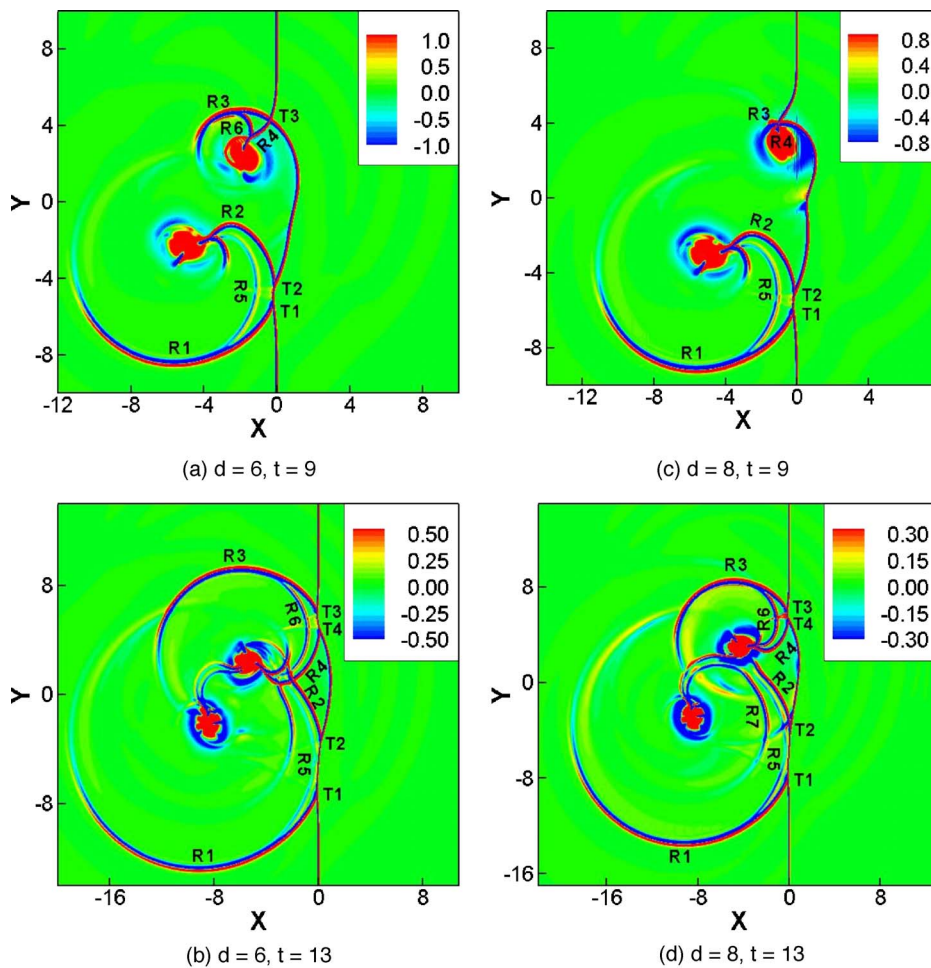


FIG. 16. (Color online) The shock structure of an oblique shock and a passing vortex pair interaction with different separation distance.  $M_s=1.2$ ,  $M_v=0.8$ ,  $\alpha=45^\circ$ ,  $L=4$ .

pair. It radiates outward from the middle of the vortex pair. The appearance of double cells is a trace of the merging result. The third sound wave [marked by  $T$  in Fig. 17(f)] and the fourth sound wave mainly result from the interaction of the deformed incident shock wave and the second vortex. They radiate outward from the center of the second vortex.

This double cell structure can be observed for a large range of  $\alpha$ . Figure 18 is the sound pressure at different angle  $\alpha$ , which ranges from  $15^\circ$  to  $75^\circ$ . For a small  $\alpha$ , the sound pressure takes the symmetric pattern of the parallel case.<sup>16,15</sup> As  $\alpha \geq 35^\circ$ , the double cell structure appears. When  $\alpha=75^\circ$ , it approaches the tandem case.<sup>16</sup> The sound wave is composed of a quadrupolar nature that is the same as that in a shock and a single vortex interaction.<sup>13,12</sup> However, there is still the double cell structure in the second sound wave.

Figure 19 is the circumferential variation of the sound pressure  $\Delta p$  for the four sound waves at  $t=15$ . The precursor is plotted along the circle  $r=14.7$  from the center of the lower vortex  $(-10.410, -1.417)$ . The second sound is plotted along the circle  $r=11.6$  from the middle point (a saddle point in the contour of the sound pressure) of the two vortices  $(-9.307, -0.0118)$ . The third and the fourth sound waves are plotted along the circles  $r=8.96$  and  $r=5.58$ , respectively, from the center of the upper vortex  $(-8.328, 1.406)$ . It is observed that the second sound wave is opposite in sign to the precursor. The circumferential variation of the sound pressure  $\Delta p$  of the third sound wave has the same sign as the

precursor and the circumferential variation of the sound pressure  $\Delta p$  of the fourth sound wave has the same sign as the second sound wave. All these four sound waves are composed of five alternating compressible and rarefaction regions. This structure is similar to that in the parallel shock and a vortex pair interaction.<sup>13,15</sup> Figure 20 shows the distribution of the sound pressure jump  $\Delta P$  against the distance from the upper and lower vortex centers to the points  $(-20.1, -12.2)$  and  $(-21.12, 8.443)$ , respectively. These two points correspond to the minimum and maximum of the precursor, respectively. The points  $A$  and  $B$  in Fig. 20 represent the double cells of the second sound wave.

In the simulation for the interaction of a shock wave and a vortex pair that is parallel to the incident shock wave, the incident shock wave touches the two vortices at the same time. The shock wave interacts with the two vortices at the same time and the sound waves generated by the interaction of the incident shock wave and two different vortices appear at same time. Hence, the flow field including sound field is symmetric. These sound waves propagate radially outward from the middle point of the vortices in the downstream of the shock wave. The merging mechanism is buried.

In the colliding case, we only observe three sound waves, which agrees with that obtained by Inoue and Hattori.<sup>13</sup> However, Pirozzoli *et al.*<sup>15</sup> observed four sound waves when they simulated in a larger computational do-

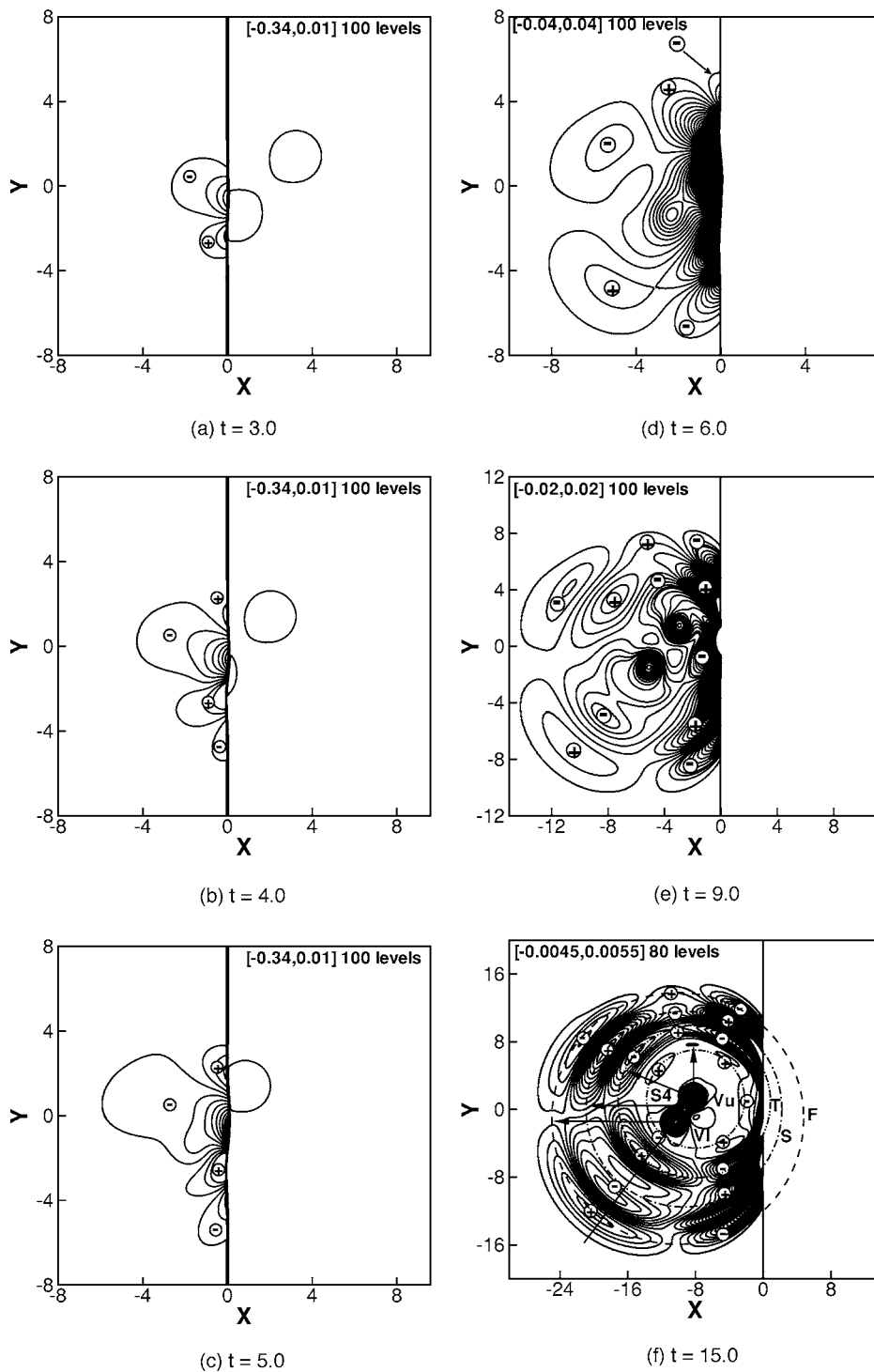


FIG. 17. The evolution of sound pressure  $\Delta p = (p - p_s) / p_s$  of an oblique shock and a passing vortex pair interaction,  $M_s = 1.2$ ,  $M_v = 0.05$ ,  $L = 4$ ,  $d = 4$ , and  $\alpha = 45^\circ$ .

main. This means that larger domain is needed to provide full information of sound waves. However, the basic mechanism of sound generation is not affected.

## 2. The effect of vortex coupling

When the vortex pair is strong, the vortex coupling effect is significant. The free evolution of the vortex coupling also generates sound waves.<sup>15</sup> These sound waves propagate radially outward from the middle point of the vortices in the right region of the shock wave. As these sound waves im-

pinge on the incident shock wave, the transmitted sound wave merges together with the sound wave generated by the interaction of the incident shock wave and the vortex pair.

Figure 21 is an example of the sound pressure of  $M_s = 1.2$  and  $M_v = 0.25$  at  $t = 15$ . Both the initial distance and the separation distance are 4. The angle  $\alpha$  is  $45^\circ$ . We observe that the precursor has two parts: the front and the peak. The front is the transmitted sound wave that is generated by the process of vortex coupling. Because the initial vortex pair is close to the shock wave in our simulation, as the sound wave generated by the vortex coupling process impinges on the

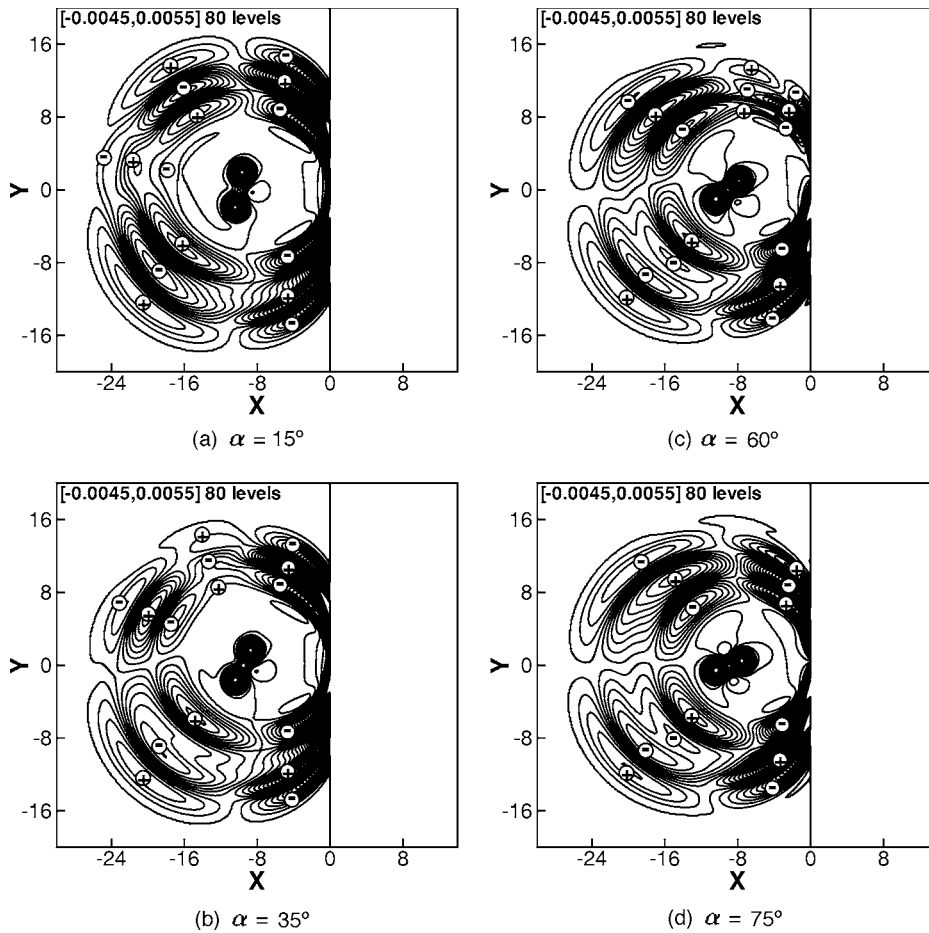


FIG. 18. Sound pressure  $\Delta p=(p-p_s)/p_s$  of an oblique shock and a passing vortex pair interaction at different angle  $\alpha$  with  $M_s=1.2$ ,  $M_v=0.05$ ,  $L=4$ , and  $d=4$ .

incident shock wave, the precursor is generated by the interaction of the incident shock wave and the vortex pair. As a result, the transmitted sound wave merges together with the precursor and becomes the front of the precursor.

In order to elucidate the mechanism of sound generation in the coupling process of the vortex pair and isolate it from that in the oblique shock and vortex pair interaction, we have studied the interaction of an oblique shock wave and a vortex pair, which is far away from the incident shock. In this case, we use the larger computational domain  $x_r=-x_l=40$ ,  $y_r=-y_l=30$ . The initial distance of the first vortex and the

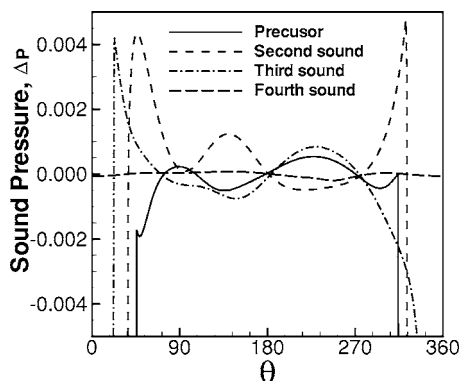


FIG. 19. The circumferential variation of the sound pressure  $\Delta p=(p-p_s)/p_s$  of an oblique shock and a passing vortex pair interaction.  $M_s=1.2$ ,  $M_v=0.05$ ,  $\alpha=45^\circ$ ,  $L=d=4$ , and  $t=15$ .

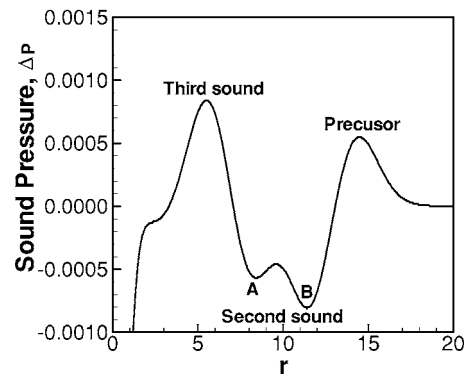
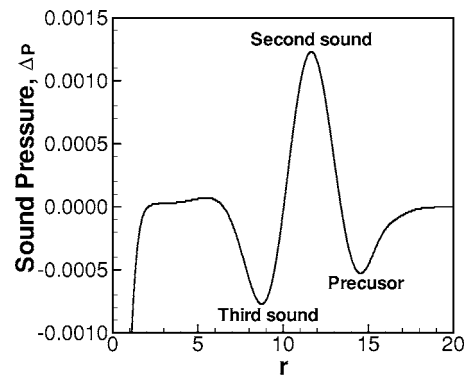


FIG. 20. The sound pressure  $\Delta p=(p-p_s)/p_s$  of an oblique shock and a passing vortex pair interaction,  $M_s=1.2$  and  $M_v=0.05$ ,  $\alpha=45^\circ$ ,  $L=d=4$ , and  $t=15$ . Top: from the center of the upper vortex to the point of minimum value of the precursor in the positive  $y$  region; bottom: the center of the bottom vortex to the point of the maximum of the precursor in the negative  $y$  region.

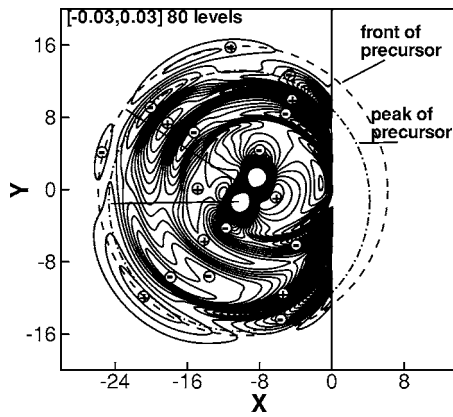


FIG. 21. The sound pressure  $\Delta p = (p - p_s) / p_s$  of an oblique shock and a passing vortex pair interaction,  $M_s = 1.2$ ,  $M_v = 0.25$ ,  $\alpha = 45^\circ$ ,  $L = d = 4$ ,  $t = 15$ .

shock wave is 20. The angle of the shock wave and the connecting line between the two vortices is  $45^\circ$ . Figure 22 is the evolution of the sound wave. In Fig. 22, the sound pressure is defined by  $\Delta p = (p - p_s) / p_s$  in the downstream region of the shock wave, while it is defined by  $\Delta p = (p - p_\infty) / p_\infty$  in the upstream of the shock wave where  $p_\infty$  represents the mean pressure in front of the shock wave. As can be seen from Fig. 22(a), the sound wave generated by the vortex coupling has a quadrupolar nature. As the vortex pair moves towards the shock wave, the sound interacts with the shock first before the vortex pair reaches the shock wave. The

transmitted sound waves propagate in the downstream of the shock wave. The shock wave is not deformed by the shock-sound interaction. This can be seen from Fig. 22(b). As the vortex pair passes through the shock wave, new sound waves are generated by the interaction of oblique shock and the vortex pair, which can be seen in Fig. 22(c). The distance between the fronts of sound wave generated by the vortex pair coupling and those in the shock vortex pair interaction approximately equals 10. Figure 22(d) shows the sound waves generated by the shock and vortex pair interaction, which has the same inner structure with that shown in Fig. 21. The only difference is that the sound wave generated by the vortex coupling process is separated from that generated by the shock vortex pair interaction when the distance between the initial vortex pair is large.

### 3. Shock sound interaction

We have observed that there are many reflected shock waves embedded in the sound field, which can be seen in the shadowgraph of  $M_s = 1.05$ ,  $1.2$ , and  $M_v = 0.8$ . These reflected shock waves can interact with the sound waves again.<sup>12</sup> As a result, the sound waves or part of the sound waves can break down and new sound waves are generated. Shock sound interaction becomes a new mechanism of sound wave generation.

In fact, there are many theoretical studies on the shock-sound interaction. Chu and Kovaszny<sup>21</sup> have shown that a

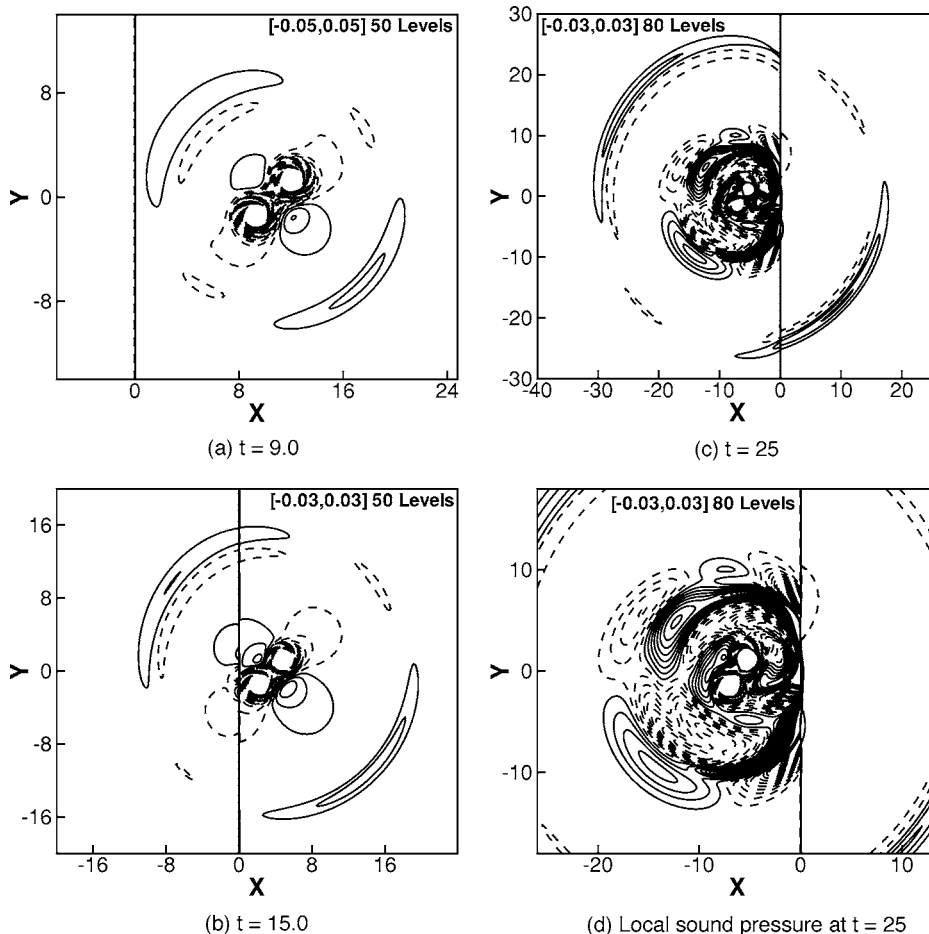


FIG. 22. The evolution of sound pressure  $\Delta p$  of an oblique shock and passing vortex pair interaction,  $M_s = 1.2$ ,  $M_v = 0.25$ ,  $\alpha = 45^\circ$ ,  $L = 20$ , and  $d = 4$ . Dashed lines represent  $\Delta p < 0$ , while solid lines represent  $\Delta p > 0$ .

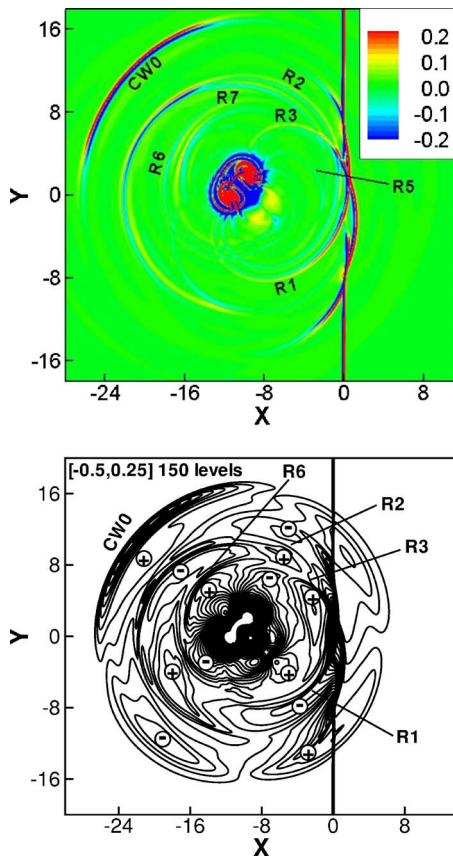


FIG. 23. (Color online) The sound pressure  $\Delta p = (p - p_s) / p_s$  of an oblique shock and a colliding vortex pair interaction,  $M_s = 1.05$ ,  $M_v = 1$ ,  $\alpha = 45^\circ$ ,  $L = d = 4$ ,  $t = 15$ . Top: shadowgraph; bottom: sound pressure.

weak disturbance in a viscous heat conducting fluid can be decomposed as the sum of three basic modes, namely, acoustic, vortical, and entropy modes. The interaction of any of these modes with a shock wave gives rise to all three disturbance modes downstream of the shock. McKenzie and Westphal<sup>22</sup> analyzed the interaction of linear waves and oblique shock waves. Formulas were derived for the amplitudes of waves that diverge from a shock wave as a result of any given incident disturbance. It is shown that the pressure amplitude and the component of the energy flux normal to the shock of a transmitted sound wave are of  $O(M^2)$  greater than those in the incident sound wave. For the incident sound wave that impinges to the shock wave near the critical angle, the ratio of the pressure amplitude of the transmitted sound wave to that of the incident one is of  $O(M^3)$ . Shu and Osher<sup>23</sup> simulated the interaction of a shock wave and a density wave. It is found that there are more complex waves behind the shock wave. This example has become a benchmark for designing and testing high order numerical schemes.<sup>24,25</sup> The interaction of a shock wave and sound wave is similar to that of a shock wave and density wave. New sound waves will be generated.

Figure 23 is an example for  $M_s = 1.05$  and  $M_v = 1.0$ . We can clearly observe the precursor. However, it is difficult to distinguish the second and third sound waves. They are broken down by the reflected shock waves. This becomes a new mechanism of sound generation of shock wave strong vorti-

ces interaction. In addition, there are new sound waves generated by the interaction of the incident shock wave and the sound waves that are generated by the vortex coupling, but we leave the study for the details of these new sound waves to the future.

#### IV. CONCLUDING REMARKS

The interaction of an oblique shock wave with a pair of vortices is systematically simulated through solving the two dimensional, unsteady compressible Navier-Stokes equations. The emphasis of the study is on the characterization of the pattern of the shock wave and the mechanism of sound generation. In particular, we have studied the effect of (1) the strengths of the shock waves and vortex pairs, (2) the direction of the self-induced velocity of the vortex pair and (3) the geometry parameters.

The results show that the interaction of an oblique shock wave and a pair of vortices has the feature of secondary interaction between the reflected shock wave or the shock focusing region, which is generated by the first interaction between the incident shock wave and the first vortex, and the upper vortex. The pattern of the shock wave is strongly affected by the direction of the self-induced velocity of the vortex. In the case of a colliding vortex pair (whose  $x$  component of self-induced velocity is in the opposite direction of the shock wave), the secondary interaction merges together with the first interaction of the deformed incident shock wave and the second vortex. The interaction has been classified into seven different types according to the different patterns of the shock waves that contain the shock focusing region, multiple shock focusing regions, and shock-shock interaction. In the case of a passing vortex pair, the secondary interaction is independent of the first interaction of the incident shock wave and the vortex pair. The interaction is classified into four types according to whether there is a secondary interaction or shock-shock interaction of the effect of vortex coupling. These shock structures are not affected by the initial distance. The separation distance influences the coupling effect. It behaves as isolated vortices if it is larger than 6.

The sound wave is generated through three different mechanisms of the interaction itself, the vortex coupling process and shock-sound interaction. The interaction of an oblique shock wave and a vortex pair generates four sound waves independent of the case of the vortex pair. The precursor is generated by the first interaction of the incident shock wave and the first vortex. It radiates outward from the center of the first vortex. The second sound wave is a merging result of the second sound wave generated by the first interaction of the incident shock wave and first vortex and the second interaction of the incident shock wave and the second vortex. It has a double cell structure in the negative  $y$  region and it radiates outward from the middle of the two vortices. The third and fourth sound waves are generated by the second interaction of the deformed incident shock wave and the second vortex.

The coupling process generates sound waves in the right region of the incident shock wave. Through the interaction

with the incident shock wave, the sound wave generated by the coupling process becomes a front of the precursor for the case in our simulation. If the initial vortex pair is far enough from the incident shock wave, they will become separated sound waves.

If the vortex pair is strong, there are many reflected shock waves that embed in the sound waves. These reflected shock waves interact with the sound waves which result in the generation of new sound waves. This is a new mechanism of sound generation. The detail of these shock-sound interactions is left for future study.

## ACKNOWLEDGMENTS

The first author was supported by the Chinese National Natural Science Foundation Grant No. 10572146. The third author was partially supported by the Chinese Academy of Sciences while he was visiting the University of Science and Technology of China (Grant No. 2004-1-8) and the Institute of Computational Mathematics and Scientific/Engineering Computing. Additional support for the third author is provided by ARO Grant No. W911NF-04-1-0291 and NSF Grant No. DMS-0510345.

<sup>1</sup>M. A. Hollingsworth and E. J. Richards, "A schlieren study of the interaction between a vortex and a shock wave in a shock tube," British Aeronautical Research Council Report No. 17985, Fluid motion subcommittee, 17985, FM 2323 (1955).

<sup>2</sup>D. S. Dosanjh and T. M. Weeks, "Interaction of a starting vortex as well as a vortex street with a traveling shock wave," *AIAA J.* **3**, 216 (1965).

<sup>3</sup>A. Naumann and E. Hermanns, "On the interaction between a shock wave and a vortex field," *AGARD Conf. Proc.* **CP-131**, 23.1 (1973).

<sup>4</sup>H. S. Ribner, "The sound generated by interaction of a single vortex with a shock wave," University of Toronto, Institute of Aerospace Studies, UTIA Report No. 61 (1959).

<sup>5</sup>H. S. Ribner, "Cylindrical sound wave generated by shock-vortex interaction," *AIAA J.* **23**, 1708 (1985).

<sup>6</sup>T. M. Weeks and D. S. Dosanjh, "Sound generation by shock-vortex interaction," *AIAA J.* **5**, 660 (1967).

<sup>7</sup>L. Ting, "Transmission of singularities through a shock wave and the

sound generation," *Phys. Fluids* **17**, 1518 (1974).

<sup>8</sup>L. Guichard, L. Vervisch, and P. Domingo, "Two-dimensional weak shock-vortex interaction in a mixing zone," *AIAA J.* **33**, 1797 (1995).

<sup>9</sup>J. L. Ellzey, M. R. Henneke, J. M. Picone, and E. S. Oran, "The interaction of a shock with a vortex: Shock distortion and the production of acoustic waves," *Phys. Fluids* **7**, 172 (1995).

<sup>10</sup>J. L. Ellzey and M. R. Henneke, "The shock-vortex interaction: The origins of the acoustic wave," *Fluid Dyn. Res.* **21**, 171 (1997).

<sup>11</sup>J. L. Ellzey and M. R. Henneke, "The acoustic wave from a shock-vortex interaction: Comparison between theory and computation," *Fluid Dyn. Res.* **27**, 53 (2000).

<sup>12</sup>S. Zhang, Y.-T. Zhang, and C.-W. Shu, "Multistage interaction of a shock wave and a strong vortex," *Phys. Fluids* **17**, 116101 (2005).

<sup>13</sup>O. Inoue and Y. Hattori, "Sound generation by shock-vortex interactions," *J. Fluid Mech.* **380**, 81 (1999).

<sup>14</sup>S. K. Lele, "Compact finite difference schemes with spectral-like resolution," *J. Comput. Phys.* **103**, 16 (1992).

<sup>15</sup>S. Pirozzoli, F. Grasso, and A. D'Andrea, "Interaction of a shock wave with two counter-rotating vortices: Shock dynamics and sound production," *Phys. Fluids* **13**, 3460 (2001).

<sup>16</sup>O. Inoue, T. Takahashi, and N. Hatakeyama, "Separation of reflected shock waves due to secondary interaction with vortices: Another mechanism of sound generation," *Phys. Fluids* **14**, 3733 (2002).

<sup>17</sup>G.-S. Jiang and C.-W. Shu, "Efficient implementation of weighted ENO schemes," *J. Comput. Phys.* **126**, 202 (1996).

<sup>18</sup>F. Grasso and S. Pirozzoli, "Simulations and analysis of the coupling process of compressible vortex pairs: Free evolution and shock induced coupling," *Phys. Fluids* **13**, 1343 (2001).

<sup>19</sup>F. Grasso and S. Pirozzoli, "Shock-wave-vortex interactions: shock and vortex deformations, and sound production," *Theor. Comput. Fluid Dyn.* **13**, 421 (2000).

<sup>20</sup>B. Sturtevant and V. A. Kulkarny, "The focusing of weak shock waves," *J. Fluid Mech.* **73**, 651 (1976).

<sup>21</sup>B. T. Chu and S. G. Kovasznay, "Non-linear interactions in a viscous heat-conducting compressible gas," *J. Fluid Mech.* **3**, 494 (1958).

<sup>22</sup>J. F. McKenzie and K. O. Westphal, "Interaction of linear waves with oblique shock waves," *Phys. Fluids* **11**, 2350 (1968).

<sup>23</sup>C.-W. Shu and S. Osher, "Efficient implementation of essentially non-oscillatory shock capturing schemes," *J. Comput. Phys.* **77**, 439 (1988).

<sup>24</sup>S. Pirozzoli, "Conservative hybrid compact-WENO schemes for shock-turbulence interaction," *J. Comput. Phys.* **178**, 81 (2002).

<sup>25</sup>N. A. Adams and K. Shariff, "A high-resolution hybrid compact-ENO scheme for shock-turbulence interaction problems," *J. Comput. Phys.* **127**, 27 (1996).